Response to the comments of Referee #1:

The paper studied a regional ozone pollution synthetically affected by subtropical high and typhoon system in the Yangtze River Delta region, China. The o3 pollution has been raised wide attention, and it's an interesting investigation and the manuscript is well written, the discussions are comprehensive, and the results are described clearly. I think that this paper deserves to be published in ACP.

We would like to thank the referee for the valuable and affirmative comments of our manuscript.

Response to the comments of Referee #2:

This study discussed the combined effects of two synoptic systems on O3 pollution in eastern China city clusters. Subtropical high was identified as the main cause of O3 episode, which was also influenced by a typhoon system. The case study was meaningful and to some extend representative of the typical O3 episodes in summer of eastern and southern China.

However, many scientific and technical problems must be addressed before this paper is reconsidered to be accepted.

We appreciate the referee for the valuable and constructive reviews of our manuscript. We carefully revise the manuscript based on the following comments.

Scientific problems:

1. Both VOCs and NOx are key precursors of O3, the authors only mentioned and analyzed the patterns of NO2 and CO. It was not enough to explain the spatial characteristics of O3 pollution. Even so, the authors did not well establish the possible relationships between O3 and NO2 and CO. Then, why to show them in Table 2. Suggest to add more O3 precursors and deepen the discussions.

Thanks for the constructive comment. We agree that NO_x and VOC are the most important precursors of O_3, and the possible relationships between O_3, VOC and NO_x should be well established. So following the suggestion, the observed VOC records at an urban site in Shanghai (SAES, 31.17°N, 121.43°E) is added, and Section 3.1 is rewritten.

In the new revised manuscript, the time series of VOCs is shown in the new Fig. 3. The brief description of the site and the measurement method for VOC is added on lines 125-131. Meanwhile, in order to better discuss the O_3-VOCs-NO_x relationship and reflect the basic characteristics of this O_3 pollution episode, the temporal variations of NO_2 in Shanghai, Hangzhou and Nanjing are also provided in the new Fig. 3. Based on the new Fig. 3, the temporal variations of O_3 and its precursors (NO_2 and VOC), as well as their internal links, are discussed. Please see lines 293-306 in the revised manuscript.

In the rewritten Section 3.1, we focus on the possible relationships of O_3, VOC and NO_x. So, the statistic data for CO in Table 2 and the simple discussion in the original manuscript are deleted. We have tried to find more VOC data to deepen our discussion. Unfortunately, only the records in Shanghai are available in this study, because the data of VOC in the Yangtze River Delta region are very limited and hard to get.

2. Page 17, lines 410-413, the explanation to biases of O3 and NO2 were not convincing. The first sentence was meaningless. Although the second sentence described a common sense, it was not responsible for the discrepancies between simulation and observation. Note that the real conditions of O3 photochemistry are also non-linear.
Thanks for the constructive comment. We carefully analyze the biases of O_3 and NO_2, and rewrite the words on lines 410-413 in the original manuscript.

In the new revised manuscript, we present three causes resulting in the biases, including the uncertainties in emissions of ozone precursors ("higher estimation of NO_x emission in Shanghai leads to higher NO_2 and lower O_3 predictions, while lower NO_x estimations in Nanjing and Hangzhou result in lower NO_2 and higher O_3 modeling results"), the overestimations in WS_{10} and the negative biases in T_2, and some imperfections in the nonlinear chemical reactions coupled in CMAQ (especially the nocturnal chemistry). Please see lines 451-461 of the new revised manuscript.

3. Throughout the paper, the authors did not say why to select these four cities? Particularly for Wuxi, it was not a provincial capital or an extremely polluted city according to the information the authors provided.
Thanks for the constructive comment.

In the original manuscript, the meteorological and air quality observation data at the observation sites in Shanghai (SH, 31.40°N, 121.46°E), Hangzhou (HZ, 30.23°N, 120.16°E), and Nanjing (NJ, 32.00°N, 118.80°E) are used to validate the reliability of simulation by WRF/CMAQ. Unfortunately, we cannot get the meteorological records at the sites in Wuxi (31.62°N, 120.27°E). So, only the observed air quality data are adopted to evaluate the performance of CMAQ. Additionally, to reveal the roles of the individual physical and chemical processes involved in O_3 formation, we present the results of the IPR analysis for the typical cities such as Shanghai, Nanjing and Hangzhou. These cities (Shanghai, Nanjing, Hangzhou, and Wuxi) are all highly urbanized and industrialized, and suffer from severe O_3 pollution. For Shanghai, Nanjing and Hangzhou, they are provincial capitals and typical mega cities in YRD, and they also represent the cities in Southeast Coastal Region (SCR), Northwestern Inland Region (NIR), and Central Inland Region (CIR). For Wuxi, it is located between Shanghai and Nanjing, and also close to the Taihu Lake. So, we chose these cities for model validation and further analysis.

We are sorry that we did not emphasis why to select these cities in the original manuscript. In the new revised manuscript, we provide more information in Methodology to indicate our consideration. We rewrite the section “2.1 Observed meteorological and chemical data”, and revise some words in the section “2.3 Integrated Process Rate (IPR) analysis method” and the section “2.4 Evaluation method”. The comparison between the observed and the simulated O_3 concentrations in Wuxi is just a supplement for the evaluation of CMAQ. On account that the comparisons in Shanghai, Nanjing and Hangzhou are enough to prove the good performance of our simulations, the comparison for O_3 in Wuxi is deleted. Please see new figure 6 and lines 440-467 in the revised manuscript.

4. Why were the modellings of wind speed and direction not validated with the observation data? They are closely related to the transport processes.

Thanks for the constructive comment. We agree that the wind components "are closely related to the transport processes", and the modeling results of wind should be "validated with the observation data".

In the new revised manuscript, the validation for the modeling results of wind speed and direction is added in Section 4.1. Please see lines 417-425 and Table 3 of the revised manuscript.

5. The northwest movement of high O3 centers from 10 to 12 Aug. was not obvious. On the basis of Fig. 6, the center located at around 34N, 34N and 33N on these three consecutive days. Clarify and revise the discussions accordingly.

Thanks for the constructive comment. According to the suggestion, in order to clarify the northwest movement of high O_3 centers from 10 to 12 Aug., we replace the old Fig. 6 in the original manuscript by the new Fig. 7. The new Fig. 7 in the revised manuscript presents the daytime vertical wind velocity and the vertical distribution of O_3 from 116.5°E to 122.9°E along the latitude of 31.40°N (where Shanghai is located). Fig. 7d-f clearly show that the high value center of O_3 concentrations (above 90 ppb) moves westwards during August 10-12, implying that the peripheral circulation of Typhoon Utor can drive the air from the coastal areas to the inland areas. Accordingly, we revise the discussions. Please see lines 476-507 of the new revised manuscript.

6. What was meant when vertical diffusion was used? How to explain diffusion process aggravated O3 pollution? Whether it was accurate to use vertical diffusion if the downward air flow transported high O3 to the surface.

It is clear that due to the downward airflows (the upper parts of Fig. 7 in the new revised manuscript) dominated by the subtropical high and the typhoon system, the YRD region is under the stable, fine and hot weather condition, and the high concentrations (> 60 ppb) of ozone usually appear from the surface to 1.5 km height. However, as shown in Fig. 7 and 8 (revised in the new manuscript), the near-surface vertical velocity is much lower than that of higher altitudes. Especially in the planetary boundary layer near cities (< 1 km), lots of zero-velocity lines appear near the ground (Fig.8). This phenomenon may be related with the upward airflow caused by Urban Heat Islands. Thus, the maximum centers of O_3 occur near the surface below 500 m, and the vertical diffusion process plays a more important role in the accumulation of surface O_3 than the advection process. The role of vertical diffusion process in the O_3 episode is similar to that reported by Zhu et al. (2015).

Reference: Zhu, B., Kang, H. Q., Zhu, T., Su, J. F., Hou, X. W., and Gao, J. H.: Impact of Shanghai urban land surface forcing on downstream city ozone chemistry, J Geophys Res-Atmos, 120, 4340-4351, 10.1002/2014JD022859, 2015.

The above explanations are also added in the new revised manuscript to avoid the confusion from readers. Please see lines 476-558.

7. Page 23, lines 541-549, evidences need to be provided to confirm whether NJ was influenced by typhoon.

Thanks for the constructive comment.

Shanghai and Hangzhou are the cities more close to the sea, so they are easily affected by the typhoon system. Before August 13, O_3 concentrations in these cities exceed the national O_3 standard because of the synthetic effects of subtropical high and typhoon system. After August 13, the YRD region is totally under the control of the typhoon system, and thereby the hot weather is relieved and the O_3 pollution is mitigated. But for Nanjing, because it is far away from the coastal areas, it is hardly affected by the downward flow in the typhoon periphery. As shown in Fig.2 and Fig.8, the concentration of O_3 in Nanjing does not exceed the national O_3 standard. The increase of O_3 in Nanjing on August 12 (Fig.8c) should mainly be caused by the local photochemical reactions because the vertical movement below 2 km above Nanjing is dominated by upward airflows. In Fig. 9c, the IPR analysis also shows that Nanjing is not easily affected by the peripheral circulation of Typhoon Utor. After August 14 (the typhoon system significantly weakens the high pressure system), however, the decrease of O_3 concentration in Nanjing is influenced by the surface wind brought by the typhoon system.

According to this suggestion, we add more evidences in Fig. 8, including the temporal variations of the vertical wind velocity and the vertical distribution of O_3 above Hangzhou and Nanjing during August 7 to 12 2013. We also add some words (as shown above) to deepen our discussion. Please see lines 538-543 and 611-620 of the new revised manuscript.

8. In the section of process analyses, the observed and simulated weather conditions in terms of spatial and temporal patterns should be provided to aid the analyses.

Thanks for the constructive comment. We have added the relevant analysis in Section 4.3. Please see lines 562-610 of the new revised manuscript.

9. Page 25, lines 586-591, why see-land breeze contributed positively to land O3 and negatively to oceanic O3? More supporting information are needed, such as the distribution map of O3 and wind fields.

Thanks for the constructive comment. On account of the high-pressure system and so-caused sinking airflows in the YRD region, the background wind is relatively weak in comparison to the local atmospheric circulation, thus the sea breeze can easily bring more generated O_3 to the shore. We add some discussion in Section 4.3.2. Please see lines 662-665 of the new revised manuscript.

10. Subtropical high is a common weather system dominating East Asia region in summer. Why did it only cause O3 episode in this period? Whether the effect was strengthened by the typhoon? On one hand, in the typhoon periphery, the strong downward flow stimulates O3 formation and suppresses air pollutants diffusion. On the other hand, had typhoon brought dirty air to the region from inland cities? Overall, the process analyses need to be more comprehensive. During the episode, when the subtropical high dominated and when typhoon dominated? Their combined

effect was promotion or offset?
Thanks for the constructive comment.

Although Western Pacific subtropical high (WPSH) is a normal influential system for the East China region in summer, but the WPSH is stronger and extends much farther west than normal in this period. The anomaly of the WPSH is the major and direct impacting factor for the hot weather (Peng et al., 2014). Besides, this O_3 episode is also influenced by the typhoon system. In the typhoon periphery, the strong downward flow may suppress air pollutants diffusion and cause contamination accumulation. It is not obvious that the typhoon brought dirty air to the region from inland cities. Instead, the clean marine inlet air brought by typhoon is advantageous to the dilution and diffusion of pollutants after the O_3 episode. We add the above explanation in the new revised manuscript.

To make the process analyses more comprehensive and answer the questions of reviewers, we rewrite the section 4.3.2 and new Fig. 11 in the new revised manuscript. Fig. 11 shows the differences of the contributions of main processes between the period of August 7-9 and August 10-12, which can quantitatively evaluate the role of the typhoon system in this severe high O_3 episode. It is clear that the abnormally strong WPSH dominated during the whole O_3 episode. Meantime, from August 10 to 12, the YRD is influenced by the typhoon system as well, because the changes in the contributions of VDIF, CHEM, DDEP, and TADV exhibit a similar spatial pattern with the high values mostly concentrating in the southeast coastal areas. Their combined effect is promoted during August 10 to 12.

Reference: Peng, J. B.: An Investigation of the Formation of the Heat Wave in Southern China in Summer 2013 and the Relevant Abnormal Subtropical High Activities, Atmospheric & Oceanic Science Letters, 7, 286-290, 2014.

Technical problems:

1. Too many grammatical errors in this paper, e.g. 1, line 15 “is detected”, line 16, exceeding”, “reaches”, line 22 “abnormal strong”, line 25 “worse air pollution”. I cannot list all of them. Strongly suggest to correct the errors with the aid of a professional language correcting company.

Sorry for these grammatical errors in the original manuscript. The errors listed above are corrected as follows.

The words “is detected” on line 14 of the original manuscript are revised to “was detected”. Please see line 13 in the new revised manuscript.

The word “exceeding” on line 16 of the original manuscript is revised to “exceeded”. Please see line 15 in the new revised manuscript.

The words “abnormal strong” on line 22 of the original manuscript are revised to “abnormally strong”. Please see line 21 in the new revised manuscript.

The words “worse air pollution” on line 25 of the original manuscript are revised to “worse air quality”. Please see line 24 of the new revised manuscript.

Additionally, the authors asked an English native speaker (named Josh Powell from Georgetown University) to help improving the English.

2. Define the abbreviations at their first appearances, e.g. WRF-CMAQ.
Thanks for the constructive comment.

As suggested above, "CMAQ" on line 27 (where "CMAQ" occurs for the first time) of the original manuscript is replaced by "the Community Multi-scale Air Quality (CMAQ) Model". Please see lines 26-27 in the new revised manuscript.

The words "With the aid of the WRF/CMAQ" on lines 96 (where "WRF/CMAQ" appears for the first time) in the original manuscript are rewritten as "The WRF/CMAQ model system, which consists of the Weather Research and Forecasting (WRF) model and the Community Multi-scale Air Quality (CMAQ) Model, were used to reveal the exact formation mechanism." in the new revised manuscript. Please see lines 98-101 in the new revised manuscript.

"(LST)" on line 146 (where "LST" appears for the first time) in the original manuscript is changed to "(local standard time, LST)". Please see line 164 in the new revised manuscript.

"PBL" on line 154 (where "PBL" appears for the first time) in the original manuscript is revised to "planetary boundary layer". Please see lines 172-173 in the new revised manuscript.

"USGS" on line 157 (where "USGS" appears for the first time) in the original manuscript is replaced by "United States Geological Survey (USGS)". Please see line 176 in the new revised manuscript.

The sentence "The initial meteorological fields and boundary conditions are from NCEP FNL global reanalysis data with 1° × 1° resolution" on lines 160-161 (where "NCEP" appears for the first time) in the original manuscript is rewritten as "The initial meteorological fields and boundary conditions are from 1° resolution global reanalysis data provided by National Center for Environmental Prediction (NCEP) ". Please see lines 178-180 in the new revised manuscript.

"(UTC)" on line 227 (where "UTC" appears for the first time) in the original manuscript is changed to "(Universal Time Coordinated, UTC)". Please see line 238 in the new revised manuscript.

“WRF-CMAQ” on line 642 of the original manuscript is revised to “WRF/CMAQ”. Please see line 735 of the new revised manuscript. The definition has been given at its first appearances (on lines 98-101 in the new revised manuscript).

3. Page 4, line 94, what is the knowledge gap?

“Knowledge gap” means the principle that we do not know and need to be studied. The phrase “to fill the knowledge gap” was also used in some other papers (Ding et al.,2013; Xie et al., 2016). Here, the authors wanted to express that it is worth to investigate how the subtropical high and the typhoon system affect the formation of this regional O_3 pollution, and the results will help us to understand the important factors impacting O3 formation from the regional scale.

To avoid unnecessary misunderstanding, the words “To fill the knowledge gap and better understand the important factors impacting O3 formation from the regional scale, we perform an observational analysis to identify the temporal and spatial characteristics of the episode. With the aid of the WRF/CMAQ as well as the Integrated Process Rate analysis (IPR) coupled within CMAQ, numerical simulations are conducted to provide qualitative and quantitative analysis on the contributions of individual atmospheric processes.” on lines 94-98 of the original manuscript are revised to “To better understand the important factors impacting O3 formation from the regional scale, we investigated the exact roles of these two typical weather systems in this pollution episode by using observational analysis and numerical simulations. The observational analysis was performed to identify the temporal and spatial characteristics of the episode. The WRF/CMAQ model system, which consists of the Weather Research and Forecasting (WRF) model and the Community Multi-scale Air Quality (CMAQ) Model, were used to reveal the exact formation mechanism. With the aid the Integrated Process Rate (IPR) analysis coupled in CMAQ, the qualitative and the quantitative analysis on the contributions of individual atmospheric processes were conducted as well.”. Please see line 95-103 of the new revised manuscript.

4. Past tense was suggested for the Introduction section, except for the common senses.
Thanks for the constructive comment. As suggested above, several sentences in the Introduction section are revised to use the past tense.

The words “there is” on line 92 of the original manuscript are revised to “there was”. Please see line 93 in the new revised manuscript.

The words “may be” on line 93 of the original manuscript are revised to “might be”. Please see line 94 in the new revised manuscript.

The words “we perform” on line 95 and “are conducted” on line 97 of the original manuscript are deleted. “…, we investigated …”, “The observational analysis was performed to …”, “…, were used …” and “… were conducted” are added in the new revised manuscript. Please see lines 97-103 of the revised manuscript.

5. Website references needed to be added for the citations of meteorological and air pollutants data.
Thanks for the constructive comment. The website references for the citations of the meteorological and air pollutants data are added in the new revised manuscript. For the meteorological data, “The weather charts for East Asia are accessible from Korea Meteorological Administration (http://www.kma.go.kr/chn/weather/images/analysischart.jsp)”, and “The hourly

meteorological data at the observation sites of SH (31.40°N, 121.46°E) located in Shanghai, HZ (30.23°N, 120.16°E) in Hangzhou, and NJ (32.00°N, 118.80°E) in Nanjing can be obtained from the University of Wyoming (http://weather.uwyo.edu/wyoming/)". For the air pollutant data, "The in-situ monitoring data for the hourly concentrations of O3, CO, NO2, SO2, PM2.5 and PM10 can be acquired from National Environmental Monitoring Center (NEMC) (http://106.37.208.233:20035)". Please see lines 116-118 and 132-138 in the new revised manuscript.

6. Page 9, lines 236-238, the function of water vapor and the evidence for its more abundance in Shanghai.
Thanks for this constructive comment. In the new revised manuscript, we pay more attention to the chemical relations between O_3 and its precursors. Section 3.1 is rewritten. Water vapor is not discussed, and the words on lines 236-238 of the original manuscript are changed to "It seems that O3 concentrations are higher in the cities around Shanghai, where the concentrations of O3 precursors (shown in Table 2) are more adequate as well.". Please see lines 285-287 of the new revised manuscript.

7. Page 17, line 395, WRF/CHEM or WRF-CMAQ?
Sorry for this clerical error. The word "WRF/CHEM" on line 395 of the original manuscript is revised to "WRF/CMAQ". Please see line 436 of the new revised manuscript.

8. Fig. 6, the legends need to be provided. Positive wind speeds with solid lines mean downward air flow?
Thanks for the constructive comment. The dotted lines show the negative wind speeds and represent downward airflow, while the solid lines show the positive vertical wind speeds and zero vertical velocity. In the new revised manuscript, the legends and the necessary explanation are added to Fig. 7 and 8. Please see lines 512-514 and 548-550 of the new revised manuscript.

9. Conclusion needs to be reorganized after the revision of the whole paper.
As suggested above, the conclusion is reorganized and revised after the revision of the whole paper. Please see lines 705-740 of the new revised manuscript.

Integrated studies of a regional ozone pollution synthetically affected by subtropical high and typhoon system in the Yangtze River Delta region, China

Lei Shu~~[1]~~**, Min Xie**~~[1]~~[*]**, Tijian Wang**~~[1,2]~~[*]**, Da Gao, Pulong Chen**~~[1]~~**, Yong Han**~~[1]~~**, Shu Li**~~[1]~~**, Bingliang Zhuang**~~[1]~~**, Mengmeng Li**~~[1]~~~~**, Da Gao**~~~~[1]~~

~~[1]School of Atmospheric Sciences, Nanjing University, Nanjing, China~~

~~[2]CMA-NJU Joint Laboratory for Climate Prediction Studies, Institute for Climate and Global Change Research, School of Atmospheric Sciences, Nanjing University, Nanjing, China~~

School of Atmospheric Sciences, CMA-NJU Joint Laboratory for Climate Prediction Studies, Jiangsu Collaborative Innovation Center for Climate Change, Nanjing University, Nanjing 210023, China

----

*Correspond~~ing author, +86-25-89685302~~ence to: Min Xie

~~E-mail address:~~ (minxie@nju.edu.cn)~~,~~ and Tijian Wang (tjwang@nju.edu.cn)

带格式的：无孤行控制

带格式的：无孤行控制

Abstract: Severe high ozone (O_3) episodes usually have close relations to synoptic systems. A regional continuous O_3 pollution episode ~~is~~ was detected over the Yangtze River Delta (YRD) region in China during August 7-12~~,~~ 2013, in which the O_3 concentrations in more than half of the cities ~~exceeding~~ exceeded the national air quality standard. The maximum hourly concentration of O_3 ~~reaches~~ reached 167.1 ppb. By means of the observational analysis and the ~~WRF/CMAQ~~ numerical simulation, the characteristics and the essential impact factors of the typical regional O_3 pollution ~~is~~ are integratedly investigated. The observational analysis shows that the atmospheric subsidence dominated by Western Pacific subtropical high plays a crucial role in the formation of high-level O_3. The favorable weather conditions, such as extremely high temperature, low relative humidity and weak wind speed, caused by the abnormally strong subtropical high are responsible for the trapping and the chemical production of O_3 in the boundary layer. In addition, when the YRD cities at the front of Typhoon Utor, the periphery circulation of typhoon system can enhance the downward airflows and cause ~~worse~~ ~~more serious~~worse air ~~pollution~~quality. But when the typhoon system weakens the subtropical high, the prevailing southeasterly surface wind leads to the mitigation of the O_3 pollution. The Integrated Process Rate (IPR) analysis incorporated in the Community Multi-scale Air Quality (CMAQ) Model is applied to further illustrate the combined influence of subtropical high and typhoon system in this O_3 episode. The results show that the vertical diffusion (VDIF) and the gas-phase chemistry (CHEM) are two major contributors to O_3 formation. During the episode, the contributions of VDIF and CHEM to O_3 maintain the high values over ~~10 ppb/h in Shanghai, Hangzhou, and Nanjing~~the YRD region. On August 10-~~11~~12, the cities close to the sea are apparently affected by the typhoon system, with the contribution of VDIF increasing to 28.45 ppb/h in Shanghai and 19.76 ppb/h in Hangzhou. In contrast, the cities ~~in the northwest inland area~~ far away from the sea ~~are generally under the control of the subtropical high and~~ can hardly be affected by the periphery circulation of typhoon system. When ~~the YRD region is under the control of~~ the typhoon system significantly weakens the subtropical high, the contribution values of all individual processes decrease to a low level in all YRD cities. These results provide an insight for the O_3 pollution synthetically impacted by the Western Pacific subtropical high and the tropical cyclone system.

Keyword: Ozone; subtropical high; typhoon; the Yangtze River Delta region; heat wave

1. Introduction

Ground-level ozone (O_3) is a secondary air pollutant generated by a series of complicated photochemical reactions involving nitrogen oxides (NO_x) and hydrocarbons (HC) (Crutzen, 1973; Sillman, 1999; Jenkin et al., 2000; Wang et al., 2006b; Xie et al., 2014; 2016b). Severe O_3 pollution events usually occur in the presence of sunlight and under favorable meteorological conditions, with the abundance of O_3 precursors (NO_x and HC) (Wang et al., 2006b). These O_3 pollutions in troposphere can deteriorate the air quality, and thereby cause adverse effects on human health and vegetation (Feng et al., 2003; Fann and Risley, 2013; Landry et al., 2013). Consequently, the formation mechanism and the integrated prevention of O_3 pollution are of great concern in many megacities all over the world (Xie et al., 2016b).

Over the past decades, along with the rapid industrial and economic development, many areas in China have been suffering from high levels of O_3 pollution. Especially in the most economically vibrant and densely populated areas, such as the Yangtze River Delta (YRD) region, the Pearl River Delta (PRD) region, and the Beijing-Tianjin-Hebei (BTH) area, the severe O_3 pollution episode has frequently occurred (Lam et al., 2005; Wang et al., 2006b; An et al., 2007; Chan and Yao, 2008; Duan et al., 2008; Jiang et al., 2008; Zhang et al., 2008; Guo et al., 2009; Shao et al., 2009; Ma et al., 2012) , and the background air pollutant concentrations have steadily increased (Chan and Yao, 2008; Zhang et al., 2008; Tang et al., 2009; Wang et al., 2009a; Ma et al., 2012; Liu et al., 2013). Many studies on the O_3 pollution, including satellite data analyses, field experiments, and model simulations, have been carried out over China in order to investigate the temporal and spatial characteristics of surface photochemical pollutions (Lu and Wang, 2006; Wang et al., 2006a; Tu et al., 2007; Zhang et al., 2007; 2008; Geng et al., 2008; Tang et al., 2008; 2009; Chen et al., 2009; Han et al., 2011; Ding et al., 2013; Xie et al., 2016b), nonlinear photochemistry of O_3 and its precursors (Lam et al., 2005; Ran et al., 2009; Liu et al., 2010; Li et al., 2011; Xie et al., 2014), interactions between O_3 and aerosols (Lou et al., 2014; Shi et al., 2015), the effects of urbanization on O_3 formation (Wang et al., 2007; 2009b; Liao et al., 2015; Li et al., 2016; Xie et al., 2016a; Zhu et al., 2016), and other essential impact factors (Jiang et al., 2012; Li et al., 2012; Wei et al., 2012; Liu et al., 2013; Gao et al., 2016).

The Yangtze River Delta (YRD) region is a highly developed area of urbanization and industrialization. With the accelerated economic development and remarkable increase in energy consumption, the photochemical smog with high level of O_3 concentration is becoming more and more prominent and frequent, tending to present ~~conspicuous~~ the ~~regional~~ characteristics of regional pollution (Chan and Yao, 2008; Ma et al., 2012; Li et al., 2012). Being located on the southeastern coast of China, YRD features a typical subtropical monsoon climate and is strongly affected by the Western Pacific subtropical high in summer. So, high O_3 concentrations are usually observed in late spring and summer by in-situ monitoring (Ding et al., 2013; Xie et al., 2016b). Severe high O_3 episodes usually have close relations to synoptic systems (Huang et al., 2005; 2006; Wang et al, 2006b; Jiang et al., 2008; Cheng et al., 2014; Hung and Lo, 2015). Horizontal and vertical transport processes from upwind O_3-rich air masses as well as poor atmospheric diffusion conditions can lead to the accumulation of surface O_3 concentrations and aggravating the photochemical pollution (Wang et al., 2006b). In previous studies on high O_3 pollution in the YRD region, some researchers have discussed this issue. For example, Jiang et al. (2012) investigated the spring O_3 formation over East China, and suggested that O_3 concentrations over the YRD region were transported and diffused from surrounding areas. Li et al. (20142) presented quantitative analysis on atmospheric processes affecting O_3 concentrations in the typical YRD cities during a summertime regional high O_3 episode, and found that the maximum concentration of photochemical pollutants was usually related with the process of transportation. Gao et al. (2016) evaluated the O_3 concentration during a frequent shifting wind period, and revealed that vertical mixing played an important positive role in the formation of surface O_3. However, these investigations only focused on the O_3 formation mechanism for one megacity (such as Shanghai, Nanjing and Hangzhou, etc.) or just a single station. Up to now, studies on the process analysis of high ozone episodes over the YRD are quite limited (Li et al., 2012). So, more studies should pay attention to the typical weather systems and the exact formation mechanism of the regional O_3 pollution in this region.

During August 7-12 2013, there ~~is~~ was a typical regional O_3 pollution episode in the YRD region, which ~~may~~ might be ~~combinedly~~ synthetically influenced by the Western Pacific subtropical high and Typhoon Utor. To ~~fill the knowledge gap and~~ better understand the important factors impacting O_3 formation from the regional scale, we ~~thoroughly~~ investigated the exact roles of these two typical weather systems in this pollution episode~~,~~ by using observational analysis and numerical simulations. ~~we perform an~~The observational analysis was performed to identify the temporal and spatial characteristics of the episode. ~~With the aid of~~ T~~t~~he WRF/CMAQ model system, which consists of the Weather Research and Forecasting ~~(WRF)~~ model– (WRF) and the Community Multi-scale Air Quality ~~–(CMAQ)~~ Model (CMAQ), were used to reveal the exact formation mechanism. With the aid ~~as well as~~ the Integrated Process Rate (IPR) analysis ~~(IPR)~~ coupled ~~with~~in CMAQ, ~~numerical simulations are were conducted to provide~~ the qualitative and the quantitative analysis on the contributions of individual atmospheric processes were conducted as well. ~~The results may be a great help for the prediction and the prevention of high O_3 pollution events.~~ In this paper, the brief description of observational data and model configurations are shown in Section 2. The detailed observational analysis of air quality and meteorological conditions are given in Section 3. The evaluation of model performance and the formation mechanism of O_3 explored by IPR technique are presented in Section 4. In the end, a summary of main findings is given in Section 5.

2. Methodology

2.1 Observed meteorological and chemical data

The weather charts and the observed surface meteorological records are used to analyze the synoptic systems during the episode in August 2013, as well as to evaluate the modeling results of meteorological factors. The weather charts for East Asia are accessible from Korea Meteorological Administration (http://www.kma.go.kr/chn/weather/images/analysischart.jsp). The hourly meteorological data at the observation sites of SH (31.40°N,121.46°E) located in Shanghai, HZ (30.23°N, 120.16°E) in Hangzhou, and NJ (32.00°N, 118.80°E) in Nanjing can be obtained from the University of Wyoming (http://weather.uwyo.edu/wyoming/), where 2-m air temperature, 2-m relative humidity, 10-m wind speed and 10-m wind direction are available.

The air quality observational data are used to identify the regional characteristics of the O_3 episode in August 2013and to validate the model performance for air pollutants. Fifteen cities are selected as the representative research objects to better reflect the status of O_3 pollution over the YRD region. The locations of these cities are shown in Fig. 1b, which contains Shanghai, 8 cities in Jiangsu province (Changzhou, Nanjing, Nantong, Suzhou, Taizhou, Wuxi, Yangzhou, and Zhenjiang), and 6 cities in Zhejiang province (Hangzhou, Huzhou, Jiaxing, Ningbo, Shaoxing, and Zhoushan). The in-situ monitoring data for the hourly concentrations of O_3, CO, NO_2, SO_2, $PM_{2.5}$ and PM_{10} can be acquired from National Environmental Monitoring Center (NEMC) (http://106.37.208.233:20035). The assurance/quality control (QA/QC) procedures for monitoring strictly follow the national standards (State Environmental Protection Administration of China, 2006). The hourly pollutant concentration for a city is calculated as the average of the pollutant concentrations from several national monitoring sites in that city, which can better characterize the pollution level of the city. In order to identify invalid or lacking data, a checking procedure for these data is performed following the work of Chiqueto and Silva (2010). Finally, only less than 0.2% of the primary data are ignored in the calculation. Moreover, the observed data of total VOCs (TVOC) during August 4-10 at an urban site in Shanghai (SAES, 31.17°N, 121.43°E) is also used. They are provided by Shanghai Academy of Environmental Sciences. The sampling height is about 15 m, and individual VOC species are continuously measured every 30 min by two on-line high performance gas chromatograph with flame ionization detector (GC-FID) systems (Chromato-sud airmoVOC C2-C6 #5250308 and airmoVOC C6-C12 #2260308, France). The details for measurement and QA/QC can refer to Wang et al. (2013).

The weather charts and the observed surface meteorological records are used to analyze the synoptic systems during the episode. The weather charts for East Asia are accessible from Korea Meteorological Administration (http://www.kma.go.kr/chn/weather/images/analysischart.jsp). The hourly meteorological data at the observation sites of SH (31.40°N, 121.46°E) located in Shanghai, HZ (30.23°N, 120.16°E) in Hangzhou, and NJ (32.00°N, 118.80°E) in Nanjing can be obtained from the University of Wyoming (http://weather.uwyo.edu/wyoming/), where 2-m air temperature, 2-m relative humidity, 10-m wind speed and 10-m wind direction are available.

Meteorological and air quality observation data are also used to validate the reliability of simulations in this study. Comparisons of the modeling results in the finest domain (d03) with the hourly observation data are performed in Shanghai, Hangzhou and Nanjing-, and Hangzhou. for 2-m air temperature, 2-m relative humidity, 10-m wind speed, 10-m wind direction, surface O_3 and surface NO_2. As a supplement, the modeling results and observations for the surface hourly O_3 concentrations in Wuxi are compared as well due to the fact that the meteorological data of Wuxi is unavailable from the University of Wyoming. Shanghai (31.40°N, 121.46°E) is the most populous city in China and Asia, as well asand also a global financial and transportation center. Locating to the northwest of Shanghai, Nanjing (32.00°N, 118.80°E) is the capital of Jiangsu Province and the second largest commercial center in East China. Hangzhou (30.23°N, 120.16°E) is the capital of Zhejiang Province and located to the southwest of Shanghai. These cities are the provincial capitals and the typical metropolis in the YRD region. They are highly urbanized and industrialized, and all suffer from severe O_3 pollution. Additionally, Wuxi (31.62°N, 120.27°E) is located between Shanghai and Nanjing and close to the Taihu Lake.

2.2 Model description and configurations

In this paperstudy, WRF/CMAQ, which consists of the Weather Research and Forecasting (WRF) model version 3.4.1 and the Community Multi-scale Air Quality (CMAQ) Model version 4.7.1, is applied to simulate the high O_3 episode over the YRD region in August 2013. Developed at the National Center for Atmospheric Research (NCAR), WRF is a new generation of meso-scale weather forecast model and assimilation system developed at the National Center for Atmospheric Research (NCAR). Numerous applications have proven that it shows a good performance in all kinds of weather forecasts and has broad application prospects in China (Jiang et al., 2008; 2012; Wang et al., 2009b; Liu et al., 2013; Xie et al., 2014; 2016a; Liao et al., 2014; 2015; Li et al., 2016; Zhu et al., 2016). WRF provides off-line meteorological fields as the input for the chemical transport model CMAQ. ~~The~~ CMAQ ~~modeling system~~ is a third generation of regional air quality model developed by the Environmental Protection Agency of USA (USEPA). A set of up-to-date compatible modules and control equations for the atmosphere is incorporated in the model, which can fully consider atmospheric complicated physical processes, chemical processes and the relative contribution of different species (Byun and Schere, 2006; Foley et al., 2010). CMAQ has been widely applied in China and proven to be a reliable tool in simulating air quality from city scale to meso scale (Li et al., 2012; Wei et al., 2012; Liu et al., 2013; Zhu et al., 2016).

The simulation run is conducted from 08:00 (local standard time, LST) on August 2~~nd~~ to 08:00 (LST) on August 16~~th~~ 2013, in which the first 48 h is taken as the spin-up time. Three one-way nested domains are used in WRF with a Lambert Conformal map projection. The domain setting is shown in Fig. 1. The outermost domain (domain 1, d01) covers the most areas of East Asia and South Asia, with the horizontal grids of 88×75 and the grid spacing of 81km. The nested domain d02 covers the southeastern part of China, with the horizontal grids of 85×70 and the grid spacing of 27km. The finest domain (domain 3, d03) covers the core areas of the YRD region, with the grid system of 70×64 and the resolution of 9km. For all domains, there are 23 vertical sigma layers from the surface to the top pressure of 100hPa, with about 10 layers in the planetary ~~PBL~~ boundary layer. The detailed configuration options for the dynamic parameterization in WRF are summarized in Table 1. Additionally, the SLAB scheme that does not consider urban canopy parameters is adopted to model the urban effect. In order to reflect the rapid urban expansion in the YRD region, the default United States Geological Survey (USGS) land-use archives are updated by adding the present urban land-use conditions from 500-m Moderate Resolution Imaging Spectroradiometer (MODIS) data, based on the work of Liao et al. (2014; 2015). The initial meteorological fields and boundary conditions are from 1° resolution global reanalysis data provided by National Center for Environmental Prediction (NCEP) ~~FNL global reanalysis data with 1°×1° resolution~~. The boundary conditions are forced every 6 h.

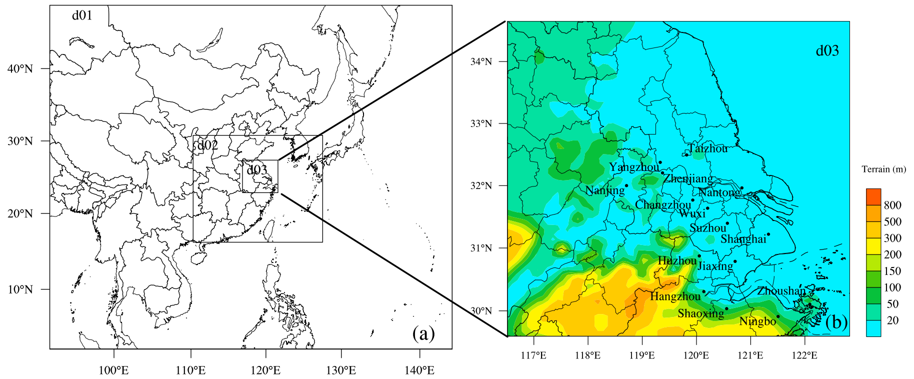

Fig. 1. Domain settings, include (a) the three nested modeling domains and (b) the nested domain 3 (d03) with the terrain elevations and the locations of 15 main cities in the YRD region.

Table 1. The grid settings and the physical options for WRF in this study.

Items	Options
Dimensions (x, y)	(88, 75), (85, 70), (70, 64)
Grid spacing (km)	81, 27, 9
Microphysics	WRF Single-Moment 5-class scheme (Hong et al., 2004)
Longwave Radiation	RRTM scheme (Mlawer et al., 1997)
Shortwave Radiation	Goddard scheme (Kim and Wang, 2011)
Surface layer	Moni-Obukhov scheme (Monin and Obukhov, 1954)
Land-surface layer	Noah Land Surface Model (Chen and Dudhia, 2001)
Planetary Boundary layer	YSU scheme (Hong et al., 2006)
Cumulus Parameterization	Grell-Devenyi ensemble scheme (Grell and Devenyi, 2002)

With respect to the air quality model, CMAQ uses the same vertical levels and the similar three nested domains as those adopted in the meteorological simulation, whereas the CMAQ domains are one grid smaller than the WRF domains. The Meteorology Chemistry Interface Processor (MCIP) is used to convert WRF outputs to the input meteorological files needed by CMAQ. The Carbon Bond 05 chemical mechanism (CB05) (Yarwood et al., 2005) is chosen for gas-phase chemistry, and the 4rd generation CMAQ aerosol module (Byun and Schere, 2006) is adopted for aerosol chemistry. The initial and outmost boundary conditions are obtained from the Model for Ozone and Related Chemical Tracers version 4 (MOZART-4) (Emmons et al., 2010), while those for the two nested inner domains are extracted from the immediate concentration files of their parent domains. The anthropogenic emissions are mainly from the 2012 ~~year~~

Multi-resolution Emission Inventory for China (MEIC) with 0.25°× 0.25° resolution, which is re-projected for the grids of China in both domains. For the grids outside of China, the inventory developed for the Intercontinental Chemical Transport Experiment-Phase B (INTEX-B) by Zhang et al. (2009) is used. The natural O_3 precursor emissions are calculated by the natural emission model developed by Xie et al. (2007; 2009; 2014), including NO from soil, VOCs from vegetations, and CH_4 from rice paddies and terrestrial plants. The biomass burning emissions are acquired from the work of Xie et al. (2014; 2016a).

2.3 Integrated Process Rate (IPR) analysis method

The CMAQ modeling system contains process analysis module (PROCAN), which consists of the Integrated Process Rate (IPR) analysis and the Integrated Reaction Rate (IRR) analysis (Byun and Schere, 2006). IPR has the capability of calculating the hourly contributions of individual physical processes and the net effect of chemical reaction compared to the overall concentrations, and thereby can determine the quantitative contribution of each process in a specific grid cell. The atmospheric processes taken into considerationconsidered in IPR include the horizontal advection (HADV), the vertical advection (ZADV), the horizontal diffusion (HDIF), the vertical diffusion (VDIF), the emissions (EMIS), the dry deposition (DDEP), the cloud processes with the aqueous chemistry (CLDS), the aerosol processes (AERO) and the gas-phase chemistry (CHEM). The IPR analysis has been widely applied to investigate the regional photochemical pollutions, and proven to be an effective tool to show the relative importance of every process and provide a fundamental interpretation (Goncalves et al., 2009; Li et al., 2012; Liu et al., 2013; Zhu et al., 2016).

In this paper, the period during from August 4- to 15 is selected for the IPR analysis. With the aid of IPR, we assess the roles of the individual physical and chemical processes involved in O_3 formation over the YRD region, and further present those in the typical cities such as (Shanghai, Nanjing and Hangzhou). Shanghai is the most populous city in China and Asia, as well as a global financial and transportation center. Locating to the northwest of Shanghai, Nanjing is the capital of Jiangsu Province and the second largest commercial center in East China. Hangzhou is the capital of Zhejiang Province and located to the southwest of Shanghai. These cities are all highly urbanized and industrialized, and suffer from severe O_3 pollution.

2.4 Evaluation method

~~Meteorological and air quality observation data are used to validate the reliability of simulation in this study.~~ Comparisons of the modeling results in the finest domain (d03) with the hourly observation data are performed ~~in Shanghai (31.40°N, 121.46°E), Hangzhou (30.23°N, 120.16°E) and Nanjing (32.00°N, 118.80°E)~~ for ~~2-m air temperature, 2-m relative humidity, surface O_3 and surface NO_2~~meteorological factors and air pollutants in Shanghai, Hangzhou, and Nanjing. ~~As a supplement,~~~~Additionally, the modeling results and observations for the surface hourly O_3 concentrations in Wuxi (31.62°N, 120.27°E) are compared as well due to the fact that the meteorological data of Wuxi is unavailable from the University of Wyoming.~~ The correlation coefficient (R), the normalized mean bias (NMB) and the root-mean-square error (RMSE) are used to evaluate the model performance. These statistic values are calculated as follows:

$$R = \frac{\sum_{i=1}^{N}(S_i - \bar{S})(O_i - \bar{O})}{\sqrt{\sum_{i=1}^{N}(S_i - \bar{S})^2}\sqrt{\sum_{i=1}^{N}(O_i - \bar{O})}} \qquad (1)$$

$$NMB = \frac{\sum_{i=1}^{N}(S_i - O_i)}{\sum_{i=1}^{N} O_i} \times 100\% \qquad (2)$$

$$RMSE = [\frac{1}{N}\sum_{i=1}^{N}(S_i - O_i)^2]^{\frac{1}{2}} \qquad (3)$$

w~~W~~here S_i ~~represents the simulated value~~ and O_i represent~~s~~ the simulated and the observed value, respectively. N means the total number of valid data. Generally, the model performance is acceptable if the values of NMB and RMSE are close to 0 and that of R is close to 1.

3. Characteristics of the continuous ozone episode

3.1 Basic characteristic of the regional ozone episode in August 2013

Fig. 2 shows the temporal variation of the hourly O_3 concentrations observed ~~by in-situ monitoring~~ in 15 typical cities over the YRD region from 00:00 (Universal Time Coordinated, UTC) ~~4~~ August 4 to 23:00 (UTC) ~~15~~ August 15 in 2013. Obviously, from August 7 to ~~August~~ 12, high O_3 concentrations over 93.5 ppb (approximately equal to the hourly national air quality standard of 200 μg/m^3 ~~for the hourly O_3 concentration~~) have been frequently recorded in 13 cities, which means O_3 concentrations in most cities over the YRD region exceed the national air quality standard. So, this high O_3 pollution episode is a typical regional O_3 pollution episode that can affect the people and the ecosystem in a large area. In general, for each city, there is a remarkable continuous growth in O_3 concentrations before the O_3 episode, followed by the lasting heavy O_3 pollution period. Though the O_3 concentrations in Shaoxing and Nanjing meet the national O_3 standard, their time series still show the similar tendency for the other cities in the same region. The excessive level of O_3 occurring in Huzhou, Jiaxing, Nantong, Yangzhou and Shanghai lasts for more than six consecutive days, reflecting the regional continuous characteristics of this O_3 pollution episode.

According to the temporal variation characteristics of O_3 illustrated in Fig. 2, the abovementioned 15 typical YRD cities can be classified into three categories: (1) the cities in the Southeast Coastal Region (SCR), including Shanghai, Suzhou, Jiaxing, Ningbo, Shaoxing, and Zhoushan; (2) the cities in the Central Inland Region (CIR), including Hangzhou, Huzhou, Wuxi, Changzhou, and Nantong; and (3) the cities in the Northwestern Inland Region (NIR), including Nanjing, Yangzhou, Zhenjiang, and Taizhou. The classification is primarily on basis of the observational facts that the maximum O_3 concentrations occur on August 10-11, 12, and 13, and begin to synchronously decrease on August 12, 13 and 14 in SCR, CIR and NIR, respectively. As shown in Fig. 2, in the Southeast Coastal Region (SCR), Zhoushan firstly exceeds the national O_3 standard on August 4, followed by Jiaxing, Shanghai, Suzhou and Ningbo. The peak hourly O_3 concentration of SCR occurs in Jiaxing on August 10, with the value up to 162.4 ppb. In the Central Inland Region (CIR), Huzhou is the first city exceeding the national O_3 standard, followed by the order of Nantong, Changzhou, Wuxi, and Hangzhou. The high-level O_3 pollution in Huzhou lasts during August 5-13. In Nantong and Changzhou, the maximum hourly O_3 concentration reaches 167.1 ppb on August 10 and 166.1 ppb on August 12, respectively. As for the Northwest Inland Region (NIR), Yangzhou, Zhenjiang, and Taizhou successively exceed the national O_3 standard. It is also noteworthy that the date when O_3 concentration exceeds the national air quality standard in coastal region is ahead of that in inland regions, so is the date of O_3 decrease. The different start time of O_3 decreasing in different regions might be related to the strong southeast wind in accordance with the movement of Typhoon Utor, which is discussed in Sect. 3.2 in detail. ~~Table 2 presents the highest and the average concentrations of O_3, as well as its precursors (NO_2 and CO), observed in these 15 cities during August 7-12 2013. The highest hourly~~

O_3 concentration occurs in Nantong with the value of 167.1 ppb, which is nearly 2 times of the national air quality standard, followed by 166.1 and 162.4 ppb in Changzhou and Jiaxing, respectively. It seems that O_3 concentrations are higher in the cities around Shanghai, where the concentrations of O_3 precursors (shown in Table 2) and the water vapor are more adequate as well. High concentrations of O_3 and its precursors imply that there may be stronger photochemical reactions in these cities.

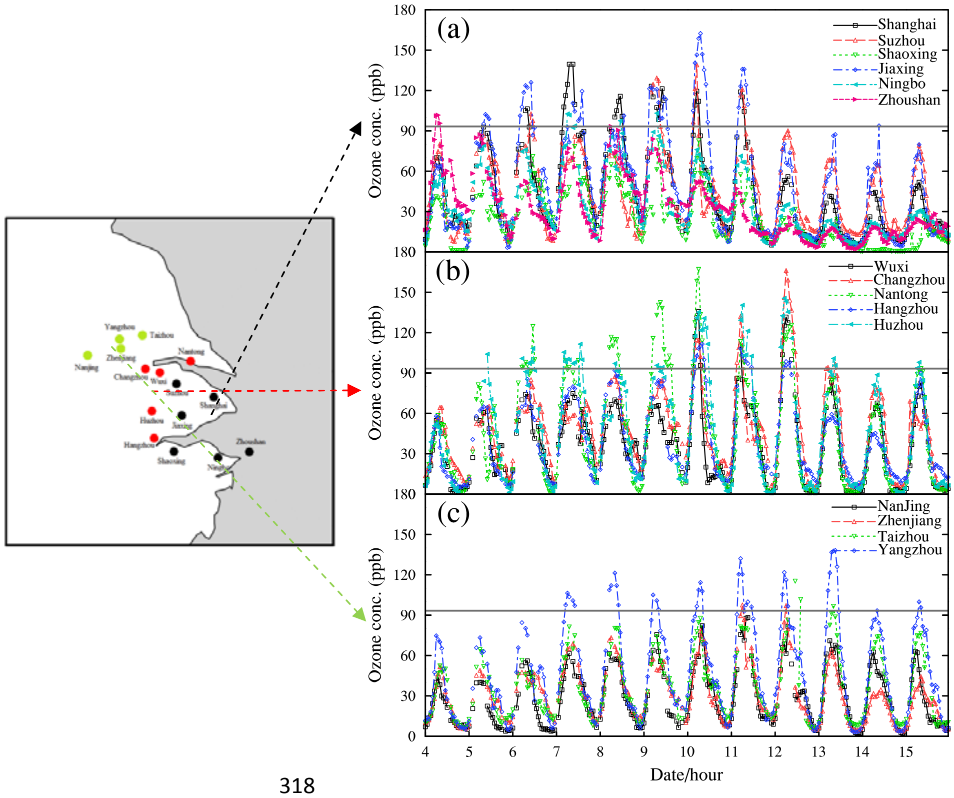

Fig. 2. The time series of the observed O_3 concentrations in 15 typical cities from August 4 to 15 August 2013 over the YRD region, which can be divided into three areas: (a) the Southeast Coast Region (SCR), including Shanghai, Suzhou, Shaoxing, Jiaxing, Ningbo, and Zhoushan; (b) the Central Inland Region (CIR), including Wuxi, Changzhou, Nantong, Hangzhou, and Huzhou; (c) the Northwest Inland Region (NIR), including Nanjing, Zhenjiang, Taizhou and Yangzhou. The gray solid lines in (a), (b), and (c) represent the national standard for the hourly O_3 concentration, which is 200 μg/m^3.

Table 2 presents the maximum and the average concentrations of O_3 and NO_2 in 15 YRD cities during August 7-12 2013. It illustrates that the mean concentrations of NO_2 in different YRD cities range from 7.7 to 24.5 ppb during the O_3 episode, indicating the heterogeneity of the spatial

带格式的：下标

distribution of O_3 precursor emissions. For O_3, the highest hourly concentration (167.1 ppb) occurs in Nantong, followed by 166.1 ppb in Changzhou and 162.4 ppb in Jiaxing. These values are all nearly 2 times of the national air quality standard. It seems that O_3 concentrations are higher in the cities around Shanghai, where the concentrations of O_3 precursors are more adequate as well. High concentrations of O_3 and its precursors imply that there may be stronger photochemical reactions.

Table 2. The maximum and average concentrations of O_3, and NO_2, and CO observed in 15 cities during August 7-12 2013 (ppb).

带格式表格

Sites		O_3		NO_2	
		Max	Mean	Max	Mean
Southeast Coast Region (CSR)	Shanghai	139.5	55.1	35.1	15.6
	Suzhou	139.1	50.9	50.6	19.7
	Jiaxing	162.4	61.1	52.1	17.1
	Ningbo	113.4	41.9	31.2	12.4
	Shaoxing	82.6	31.9	27.8	12.7
	Zhoushan	93.6	35.5	27.3	7.8
Central Inland Region (CIR)	Hangzhou	111.5	48.6	30.2	16.7
	Huzhou	145.6	57.2	43.8	20.8
	Wuxi	135.8	43.2	39.9	18.8
	Changzhou	166.1	55.7	58.4	24.5
	Nantong	167.1	56.0	48.2	20.9
Northwest Inland Region (NIR)	Nanjing	88.2	34.1	41.4	21.9
	Yangzhou	132.1	54.1	36.0	17.1
	Zhenjiang	97.5	37.7	38.5	20.1
	Taizhou	115.3	40.5	18.5	7.7

According to the temporal variation characteristics of O_3 illustrated in Fig. 2, the abovementioned 15 typical YRD cities can be classified into three categories: (1) the cities in the Southeast Coastal Region (SCR), including Shanghai, Suzhou, Jiaxing, Ningbo, Shaoxing, and Zhoushan; (2) the cities in the Central Inland Region (CIR), including Hangzhou, Huzhou, Wuxi, Changzhou, and Nantong; and (3) the cities in the Northwestern Inland Region (NIR), including Nanjing, Yangzhou, Zhenjiang, and Taizhou. The classification is primarily on basis of the observational facts that the maximum O_3 concentrations occur on August 10-11, 12, and 13, and begin to synchronously decrease on August 12, 13 and 14 in SCR, CIR and NIR, respectively. As shown in Fig. 2, in the Southeast Coastal Region (SCR), Zhoushan firstly exceeds the national O_3 standard on August 4th, followed by Jiaxing, Shanghai, Suzhou and Ningbo. The peak hourly O_3 concentration of SCR occurs in Jiaxing on August 10 with the value up to 162.4 ppb. In the Central Inland Region (CIR), Huzhou is the first city exceeding the national O_3 standard, followed by the order of Nantong, Changzhou, Wuxi and Hangzhou. The high-level O_3 pollution in Huzhou lasts from August 5th to 13th. In Nantong and Changzhou, the maximum hourly O_3 concentration reaches 167.1 ppb on August 10 and 166.1 ppb on August 12, respectively. As for the Northwest Inland Region (NIR), Yangzhou, Zhenjiang and Taizhou successively exceed the national O_3 standard. It is also noteworthy that the date when O_3 concentration exceeds the national air quality standard in coastal region is ahead of that in inland regions, so is the date of O_3 decrease. The different time of the O_3 decrease in different regions might be related to the strong southeast wind in accordance with the movement of Typhoon Utor, which is discussed in Sect. 3.2 in detail.

In general, for each city, there is a remarkable continuous growth in O_3 concentrations before the O_3 episode, followed by the lasting heavy O_3 pollution period. Though the O_3 concentrations in Shaoxing and Nanjing meet the national O_3 standard, their time series still show the similar tendency for the other cities in the same region. The excessive level of O_3 occurring in Huzhou, Jiaxing, Nantong, Yangzhou and Shanghai lasts for more than six consecutive days, reflecting the regional continuous characteristics of this O_3 pollution episode.

As for O_3 precursors, NO_2 and CO, theirthe averaged NO_2 concentrations in the YRD region during the O_3 episode show the variation range of approximately 7.7~24.5 and 460.0~1094.0 ppb, respectively(Table 2), indicating the heterogeneity of the spatial emission distribution of O_3 precursors. Besides, the relative high hourly concentrations of NO_2 show good agreements with those of O_3, implying it is one of the important O_3 precursor. Furthermore,

Fig. 3 demonstrates the hourly variations of the observed NO_2 concentrations in Shanghai, Nanjing and Hangzhou from August 4 to 15 2013, and the time series of TVOC observed at SAES in Shanghai from August 4 to 10 2013. Obviously, there are two peaks in the diurnal cycles of NO_2 and VOC at all sites, which should be related with the rush hours in cities. The photolysis of NO_2 dominates O_3-VOC-NO_x chemistry after 8:00, and thereby makes the concentrations of precursors (NO_2 and VOC) begin to decrease. Thus, the related reactions form O_3 and increase its

带格式的：正文，左，行距：1.5 倍行距，制表位：不在 35.16 字符

concentration until about 14:00. These diurnal variations of O_3 and its precursors follow the typical patterns in the polluted areas and reflect the close relationships between O_3, VOC and NO_x (Wang et al., 2013; Xie et al., 2016b). Moreover, the daily variations of NO_2 and VOC show good agreement with those of O_3. For VOC, the concentration in Shanghai largely increases since August 6, which corresponds well with the over-standard O_3 concentrations since then (Fig. 2). For NO_2, the higher values occur from August 6 to 11 in all cities, but the concentrations start to decrease on August 12, 13 and 14 in Shanghai, Hangzhou and Nanjing, respectively. It seems that the changes of O_3 precursors (NO_2 and VOC) are also affected by the movement of Typhoon Utor.

带格式的: 字体: Times New Roman, 下标

带格式的: 字体: Times New Roman, 下标

带格式的: 字体: Times New Roman, 下标

带格式的: 字体: Times New Roman, 下标

带格式的: 正文, 左, 制表位: 不在 35.16 字符

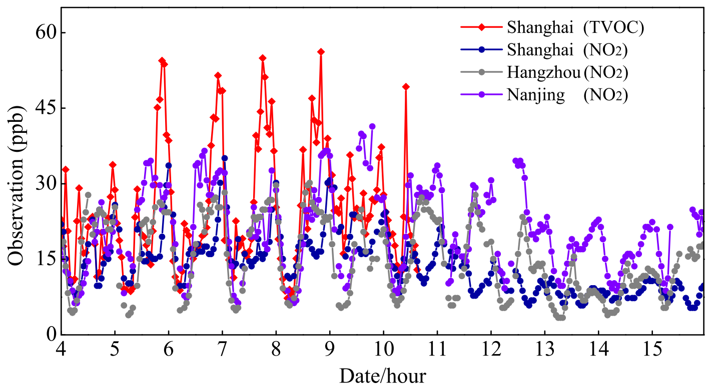

Fig. 3. Temporal variations of the observed NO_2 concentrations at Shanghai, Nanjing and Hangzhou stations from August 4 to 15 2013 and the observed TVOC concentration at SAES (31.17°N, 121.43°E) in Shanghai ~~station~~ from August 4 to ~~16:00 (UTC) August~~ 10 2013.

3.2 Meteorological condition and its effect

Favorable weather conditions have large impacts on the formation of severe O_3 pollution (Huang et al., 2005; 2006; Wang et al, 2006b; Jiang et al., 2008; Cheng et al., 2014; Hung and Lo, 2015). High-level O_3 episodes often take place in hot seasons, when the meteorological conditions with high temperature and strong solar radiation are beneficial to the photochemical reactions of O_3 (Lam et al., 2005). Fig. 4~~3~~ shows the variations of the surface meteorological parameters that are related to this photochemical pollution episode during August 4-15, including 2-m air temperature, 2-m relative humidity, 10-m wind speed and 10-m wind direction at the meteorological sites~~ of SH (31.40°N,121.46°E) located~~ in Shanghai (SH) of SCR, ~~HZ (30.23°N, 120.16°E) located in~~ Hangzhou (HZ) of CIR, and ~~NJ (32.00°N, 118.80°E) located in~~ Nanjing (NJ) of NIR .

As shown in Fig. 4~~3~~a, the hot weather at SH, HZ and NJ exists for nearly a week from August 7 to 12, with the hourly maximum temperature reaching the value over 40 ^{o}C~~°C~~. Meanwhile, the variations of 2-m relative humidity show the negative correlation with those of 2-m air temperature. The minimum 2-m relative humidity at SH and HZ occur on August 9 and August 10 respectively, with the value below 75%. These minimum values are also lower than the values before and after the O_3 episode, suggesting that high-level O_3 episodes usually occur under the weather conditions with high temperature and low humidity. The value of 2-m relative humidity at NJ is relatively higher than those at SH and HZ and remains more stable. This extremely hot and dry weather condition at SH, HZ, and NJ are successively relieved on August 12, 13 and 15, which coincide well with the reduction of surface O_3 concentrations in Shanghai, Hangzhou, and Nanjing (Fig. 2). With respect to the observed surface wind (Fig. 4~~3~~b), the 10-m wind speed at SH~~,~~ and HZ~~, and NJ~~ is comparatively lower during the period of the O_3 episode, while it is suddenly intensified after August 12. Meanwhile, the wind direction is fluctuating from August 7 to 12~~ August~~, while it maintains southeasterly wind after August 12 as well. The growth of wind speed is more distinct at SH, with the maximum value of approximately 10 m/s. The wind speed at NJ has an obviously diurnal variation from August 4 to 8, and the minimum value occurs on August 10.

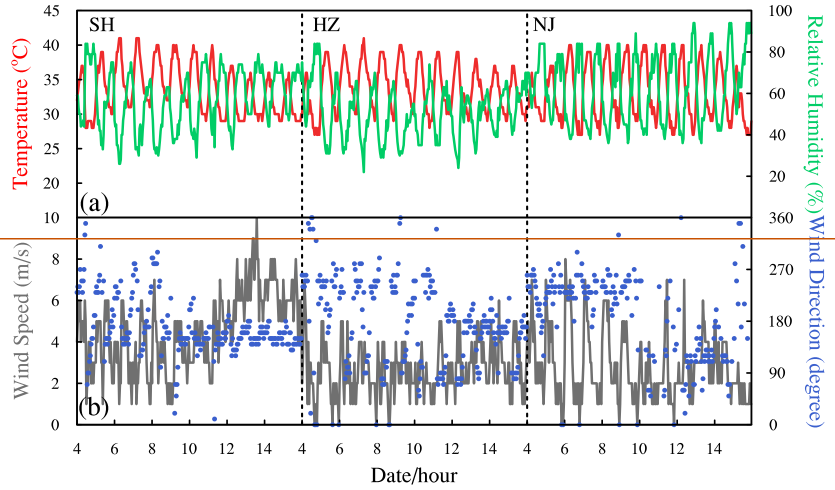

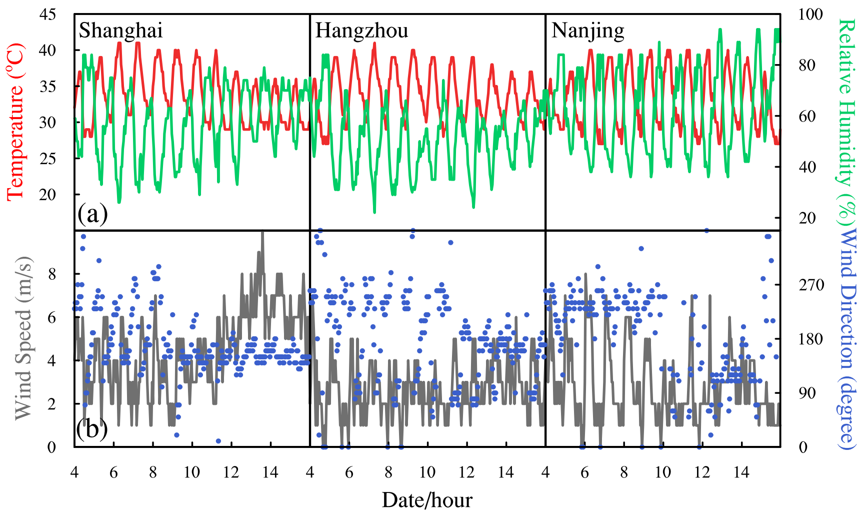

Fig. ~~4~~3. Temporal variations of the main meteorological parameters at Shanghai~~H (31.40°N,121.46°E)~~, Hangzhou~~Z (30.23°N, 120.16°E)~~ and Nanjing~~J (32.00°N, 118.80°E)~~ meteorological stations during August 4-15~~,~~ 2013~~:~~, including (a) 2-m air temperature (the red solid line) and 2-m relative humidity (the green solid line); (b) 10-m wind speed (the gray solid line) and 10-m wind direction (the blue scatter points).

Fig. ~~4~~5 displays the weather charts for the 500hPa layer over the East Asia at 00:00 (UTC) on August 6, 8, 10, and 12 ~~August~~ 2013, which can illustrate the main synoptic patterns causing the O_3 pollution. Obviously, during the period of the selected O_3 episode, the whole YRD region is under the control of the strong Western Pacific subtropical high, which is stronger and extends much farther west than normal. The anomaly of the subtropical high might be the direct and leading cause of the abnormally high temperature shown in Fig. 43a (Peng et al., 2014). The intensity of the subtropical high is usually characterized by the area index, defined as the total number of grid points that have geopotential heights of 588 decameters or greater in the region of 110-180°E and northward of 10°N. As shown in Fig. 54, the 588-decameter area covers most of southeast China, and the high pressure center (592-decameter area) is located in the southeastern coastal areas as well as the surrounding sea areas, which means the subtropical high is very intensive. This high pressure strengthens and remains over the YRD region for several days (from August 6 to 12), implying that the air subsides to the ground. The downward air acts as a dome capping the atmosphere, and helps to trap heat as well as air pollutants at the surface. Without the lift of air, there is little convection and therefore little cumulus clouds or rains. The end result is a continual accumulating of solar radiation and heat on the ground, which may greatly enhance the photochemical reactions between the abundant build-up air pollutants.

The other weather system worthy of note is Typhoon Utor (shown in Fig. 54c and d). Typhoon Utor is one of the strongest typhoons in the 2013 Pacific typhoon season, with the international code of 1311. It is formed early on August 8, develops into a tropical storm on August 9, undergoes an explosive intensification within a half of day, and achieves typhoon status on early August 10. After landing in Luzon of the Philippines on late August 11, it reemerges in the South China Sea on August 12. Typhoon Utor hits the land of Guangdong Province in China on August 14, and thereby is finally weakened into a tropical storm. In the end, it is ultimately dissipated on August 18. It was reported that ozone episodes during the hot season are usually associated with the passage of tropical cyclones close to the territory (Huang et al., 2005; Wang et al., 2006b; Jiang et al., 2008; Cheng et al., 2014; Hung and Lo, 2015). When a site is at the front of moving typhoon system, it can be controlled by the downward airflow induced by the typhoons' peripheral circulation. So, the typhoon system can cause the local weather around the site with high temperature, low humidity, strong solar radiation and small wind for a short time, before it is close enough to bring winds and rains. All these changes of meteorological conditions can significantly affecthelp to the formation ofform the severe continuous O_3 pollution (Jiang et al., 2008). In this O_3 episode, the YRD region may be influenced by the peripheral circulation of Typhoon Utor as well. Especially on August 10-11, the downward airflow in the troposphere is significantly strengthened (shown in Fig. 6 7 and detailedly discussed in Sect. 4.2), which may enhance the build-up of heat and air pollutants, and thereby result in worse air ~~pollution~~ quality shown in Fig. 2.

Moreover, ~~from August 12 to 14 (shown in Fig. 4d5d),~~ with the approaching of Typhoon Utor from August 12 to 14, the near-surface breeze over the YRD region gradually turns to be the prevailing southeasterly or southerly wind (Fig. 5d), with the highest wind speed up to 6-10 m/s in Shanghai (Fig. 4). The strengthened wind can bring the clean marine air from ocean to inland, and thereby effectively mitigate the O_3 pollution. Meantime, Typhoon Utor also gradually affects the position and strength of the Western Pacific subtropical high. As the typhoon continuously approaching and finally landing on Guangdong, the high pressure system is forced to retreat easterly and move northwards. When the high pressure center completely moves to the oceans, the YRD region is totally under the control of the typhoon system. In the end, the hot weather is relieved and the O_3 pollution is mitigated. The coastal cities in CSR are closer to the typhoon system, so they are firstly influenced during this period. Thus, the wind at SH in CSR firstly changes, followed by HZ in CIR and NJ in NIR. In the same way, 2-m air temperature and O_3 concentrations also successively decrease from southeast (SH in CSR) to northwest (NJ in NIR) owing to the scavenging effect.

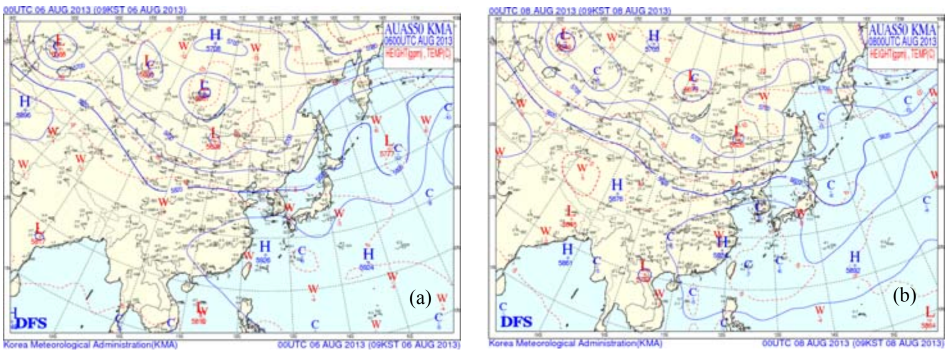

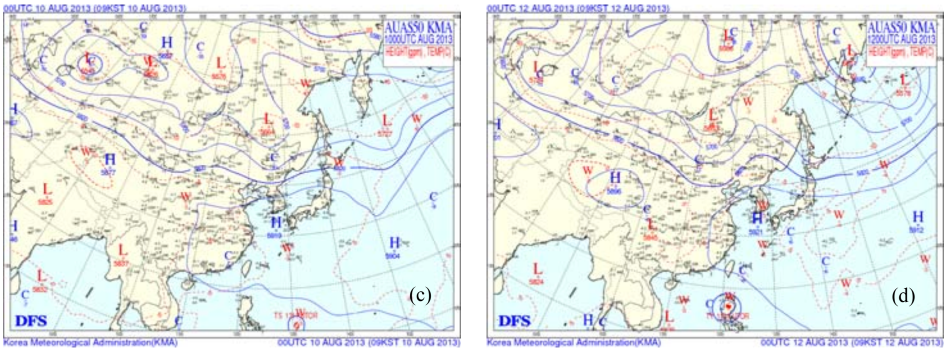

Fig. 45. Weather charts at the 500hPa layer over the East Asia at 00:00 (UTC) on (a) August 6, (b) August 8, (c) August 10, and (d) August 12 2013 (from Korea Meteorological Administration).

4 Modeling results and discussions

4.1 Evaluation of model performance

To evaluate the simulation performance, the hourly modeling results during the period of August 4-15 August 2013 are compared with the observation records. Table 3 presents the performance statistics, including the values of the correlation coefficient (R), the normalized mean bias (NMB), and the root-mean-square error (RMSE), which are all calculated for 2-m air temperature (T_2), 2-m relative humidity (RH_2), 10-m wind speed ($Wspd_{10}$), 10-m wind direction ($Wdir_{10}$), surface ozone concentrations (O_3), and surface nitrogen dioxide concentrations (NO_2) in Shanghai (SH), Nanjing (NJ), and Hangzhou (HZ).

As indicated in Table 3, the simulated results of surface air temperature and relative humidity from WRF show good correlation agreement with the observations. The highest correlation coefficient of 2-m air temperature (T_2) is found to be 0.91 at SH, followed by 0.84 at NJ and 0.80 at HZ (statistically significant at 95% confident level). The corresponding correlation coefficients for 2-m relative humidity (RH_2) are 0.85, 0.83 and 0.78, respectively. The values of RMSE for T_2 at SH, NJ and HZ are 4.15, 2.91and 3.09 ℃°C, and those for RH_2 are 19.3%, 9.41% and 13.96% respectively. However, oOur simulation underestimates T_2 and overestimates RH_2 to some certain extent, with the values of NMB for T_2 at SH, NJ and HZ being -5.68%, -5.98% and -6.53%, and those for RH_2 being 12.64%, 4.52% and 16.36%. These biases might be attributed to the uncertainty caused by the SLAB scheme, which can underestimate temperature in summer (Liao et al., 2014). , NMB (1.53%, 5.92% and 9.21% at SH, NJ and HZ site, respectively) and RMSE (2.18, 2.41 and 2.39 at SH, NJ and HZ site, respectively) are displayed concerning the wind speed

带格式的: 字体: Times New Roman, 非上标/ 下标

variable. The simulated wind speeds are a little higher than observed results, but still reasonable. Owing to the vectorial nature of wind, statistical comparisons for wind direction are shown excluding mean values of observation and simulation data, with the values of NMB at SH, NJ and HZ site being 3.53%, -1.57% and -0.13%, respectively. However, Aaccording to the relevant studies (Li et al., 2012; Liao et al., 2015; Xie et al., 2016a), this level of over- or under-estimation is still acceptable. The wind components are closely related to the transport processes. As shown in Table 3, our modeling results of wind speed and direction basically reflect the characteristics of wind fields. For 10-m wind speed (W_{spd10}), R is 077 at SH, 0.74 at NJ, and 0.75 at HZ, respectively. Though the values of NMB (1.53%, 5.92%, and 9.21%) and RMSE (2.18, 2.41 and 2.39) display that the simulated wind speeds are a little overestimated, the biases are still reasonable and acceptable. For 10-m wind direction (W_{dir10}), the simulated values also fit the observation records well, with the R values of 0.63 at SH, 0.57 at NJ and 0.58 at HZ. Comparing the mean values from SIM and OBS, we can find that WRF model generally simulates the prevailing wind direction during this period. In summary, the abovementioned performance statistics numbers basically illustrate that the WRF simulation can reflect the major characteristics of meteorological conditions during of this O_3 episode, and the meteorological outputs can be used in the pollutant concentration simulation.

Table 3. Comparisons between the simulations and the observations at Shanghai, Nanjing and Hangzhou stations during August 4-15 2013.

Sites [a]	Vars [b]	Mean		R^e	NMB [f]	RMSE [g]
		OBS [c]	SIM [d]			
SH	T_2 (°C)	33.27	31.38	0.91	-5.68%	4.15
	RH_2 (%)	57.91	65.23	0.85	12.64%	19.3
	$Wspd_{10}$ (m s^{-1})	4.59	4.66	0.77	1.53%	2.18
	$Wdir_{10}$ (°)	176.34	182.57	0.63	3.53%	41.44
	O_3 (ppb)	87.77	82.5	0.81	-6.00%	38.79
	NO_2 (ppb)	29.01	38.25	0.54	31.85%	28.95
NJ	T_2 (°C)	32.95	30.98	0.84	-5.98%	2.91
	RH_2 (%)	63.28	66.14	0.83	4.52%	9.41
	$Wspd_{10}$ (m s^{-1})	3.21	3.4	0.74	5.92%	2.41
	$Wdir_{10}$ (°)	197.68	194.58	0.57	-1.57%	71.19
	O_3 (ppb)	69.7	78.15	0.81	12.12%	36.8
	NO_2 (ppb)	41.44	40.09	0.61	-3.26%	22.4

	T_2 (°C)	33.25	31.08	0.8	-6.53%	3.09
	RH_2 (%)	52.76	61.39	0.78	16.36%	13.96
HZ	$Wspd_{10}$ (m s^{-1})	3.04	3.32	0.75	9.21%	2.39
	$Wdir_{10}$ (°)	186.45	186.2	0.58	-0.13%	69.44
	O_3 (ppb)	76.57	84.51	0.83	10.37%	33.95
	NO_2 (ppb)	31.06	27.21	0.66	-12.40%	16.86

[a] Sites indicates the city where the observation sites locate, including Shanghai (SH), Nanjing (NJ), and Hangzhou (HZ); [b] Vars indicates the variables under validation, including 2-m air temperature (T_2), 2-m relative humidity (RH_2), 10-m wind speed ($Wspd_{10}$), 10-m wind direction ($Wdir_{10}$), ozone (O_3), and nitrogen dioxide (NO_2). The words between the parentheses behind variables indicate the unit; [c] OBS indicates the observation data; [d] SIM indicates the simulation results from WRF/CMAQ~~/Chem~~; [e] R indicates the correlation coefficients, with statistically significant at 95% confident level; [f] NMB indicates the normalized mean bias; [g] RMSE indicates the root-mean-square error.

Fig. ~~5~~ 6 shows the comparisons between the modeling results from CMAQ and the observed hourly concentrations of O_3 in Shanghai, Nanjing, and Hangzhou ~~and Wuxi~~ during August 4-15 ~~August~~ 2013. Obviously, the observations and the simulated results present reasonable agreement at each site, with the correlation coefficients of 0.81 to 0.83, NMB of -6% to 12.12%, RMSE of 33.95 to 38.79 ppb. Moreover, the simulation also reproduces the diurnal variation of O_3, which shows that the concentration reaches its maximum at around noon time and gradually decreases to its minimum after midnight. With respect to the O_3 precursor, comparisons of NO_2 concentrations between simulation results and observations show that the correlation coefficient at each city is about 0.6 (given in Table 3), which further prove that the process of O_3 formation is captured reasonable well over the YRD region and throughout the episode. However, CMAQ overestimates NO_2 and underestimates O_3 in Shanghai, while underestimates NO_2 and overestimates O_3 in Nanjing and Hangzhou. These biases of O_3 and NO_2 ~~can~~ should mainly be attributed to the uncertainties in emissions of O_3 precursors (NO_x and VOC_s) (Li et al., 2012; Liao et al., 2015; Xie et al., 2016). Because of the VOC-sensitive O_3 chemistry in the daytime and NO_x titration at night in the YRD region (Xie et al., 2014), higher estimation of NO_x emission in Shanghai may lead to higher NO_2 and lower O_3 predictions, while lower NO_x estimations in Nanjing and Hangzhou may result in lower NO_2 and higher O_3 modeling results. ~~Trelated with O_3 precursor emissions, meteorology, and observation deviation (Li et al., 2012). In addition, note that this work is based on the 2012 emission scenario, while the simulation is conducted for a certain period in 2013 with~~

带格式的：下标
带格式的：下标
带格式的：下标
带格式的：下标
带格式的：下标
带格式的：下标
带格式的：下标
带格式的：下标
带格式的：下标

~~the anthropogenic emission inventory not updated. The uncertainties in emissions of ozone precursors (NOx and VOCs) may cause these biases as well (Liao et al., 2015; Xie et al., 2016).~~ he undervalued NO_2 and overvalued O_3 in Nanjing and Hangzhou ~~These underestimates should~~can also be related with the ~~increasing~~overestimations in~~of~~ WS_{10} and the negative biases in T_2. Moreover, the uncertaint~~y~~ies in nonlinear chemical reactions coupled in CMAQ may also have important effects on model predictions. For example, the modeling results cannot catch the low O_3 values observed at night in Nanjing ~~(Fig. 64b),~~and Hangzhou (Fig. 64~~c~~)~~ and Wuxi (Fig. 46d)~~, implying there may be some imperfections in the nocturnal chemistry of CMAQ. Nevertheless, the performance of CMAQ model is comparable to the other applications (Goncalves et al., 2009; Li et al., 2012; Zhu et al., 2016). Compared to these previous related studies, the simulation in this study attains an acceptable and satisfactory result. Thus, the consistency of simulation and observation demonstrates that the modeling results are capable of capturing and reproducing the characteristics and changes of photochemical pollutants, and can be used to provide valuable insights into the governing processes of this O_3 episode.

带格式的：下标

带格式的：下标

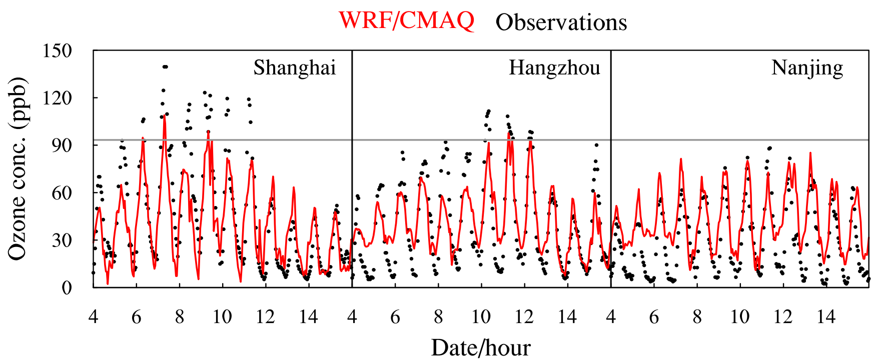

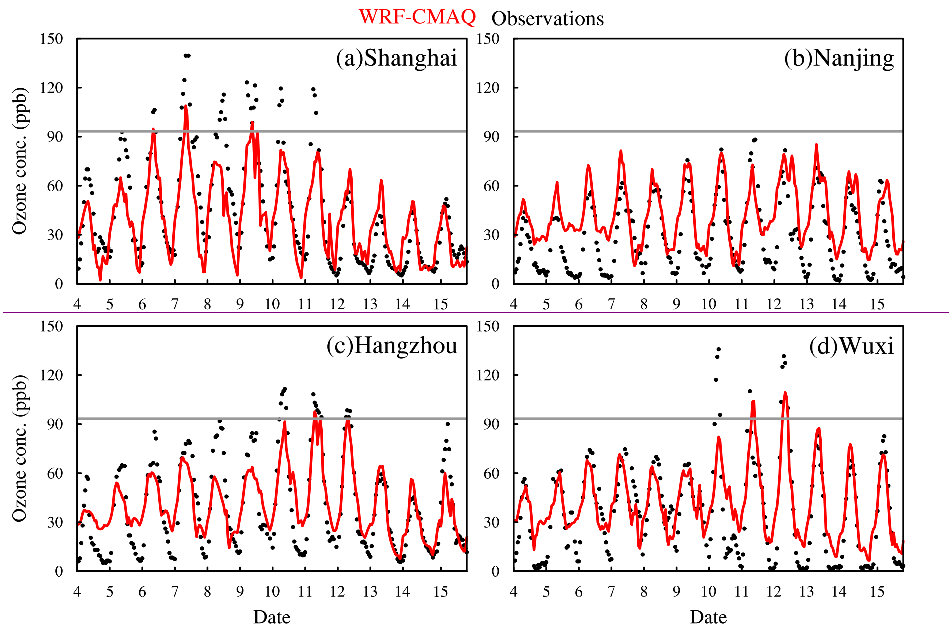

Fig. 6~~5~~. Hourly variations of the observed and the simulated O_3 concentrations in ~~(a)~~ Shanghai~~ (SH)~~, ~~(b)~~ Nanjing~~ (NJ)~~, ~~(c)~~and Hangzhou~~ (HZ), and (d) Wuxi~~. ~~In (a), (b), (c), and (d), t~~The red solid lines show the modeling results, the black dot lines give the observations, and the solid gray lines represent the national standard for the hourly O_3 concentration, which is 200 μg/m^3.

4.2 Characteristics of the vertical airflows

Fig. ~~6~~7 presents the daytime vertical wind velocity as well as the vertical distribution of O_3 concentrations from ~~29.67°NE to 34.76°EN during August 7-12 2013. Along the vertical cross-section, the values from 118°E to 122°E are averaged in the meridional direction. Moreover, Fig. 8 displays the daytime vertical wind velocity and vertical distribution of O_3 concentrations from~~ 116.5°E to 122.9°E ~~in the zonal direction~~along the latitude of 31.40°N~~,~~ (where Shanghai ~~site~~ is located) ~~lies~~ during August 7-12 2013. The simulation results clearly illustrate that there are strong downward airflows over the YRD region during the period of the regional high-level O_3 pollution, which can be attributed to the fact that these areas are under the control of the subtropical high and the sinking airflow is predominant (as discussed in Sect. 3.2).

From August 7 to 9 ~~August~~ 2013~~ (shown in Fig. 6a7a-c and 8a-c)~~, except for the mentioned regional sinking airflows~~, which are related with urban heat islands,~~ continually occurring at the lower atmospheric layers (< 2 km) along the vertical cross-section of Hangzhou (HZ)~~ - Shanghai (SH)~~ - Nanjing (NJ). These circulations are related with urban heat islands. Usually high pressures are accompanied by more stagnant and fair dry weather, so the upward and the downward flows caused by urban-breeze circulations can easily appear in the urban areas~~ of SH, HZ, and NJ~~. ~~With respect to~~For the vertical distribution of O_3~~ in the meridional direction (Fig. 7a-c)~~, its high concentrations (> ~~60~~ 50 ppb) generally ~~usually~~ appear from the surface to 1.5km height above the cities~~, with the maximum values over 70 ppb in and around cities. While in the zonal direction of 31.40°N (Fig. 8a-c), high O_3 centers (> 90 ppb) appear near the surface in the southeast coastal region~~. As discussed in Sect. 3.2, ~~induced by the regional sinking airflows,~~ air pollutants ~~are~~ tend to be trapped on the ground due to the regional sinking airflows. Moreover, the local circulations over the cities~~ (Fig. 6)~~ make the urban areas to be the convergence zones, and thereby more air pollutants can be accumulated in and around these cities. Under the weather conditions induced by the subtropical high, such as high air temperature, stronger solar radiation and less water vapor, the chemical reactions between the build-up air pollutants can be enhanced to form the high-level O_3 pollution. Additionally, Fig. 7a-c also show that there are maximum O_3 concentrations (> 90 ppb) occurring near the surface in and around SH. This phenomenon should be explained by the fact that the coastal city (SH) is firstly affected by Typhoon Utor

带格式的：下标

~~However, f~~From August 10 to 12, with the approaching of Typhoon Utor, the vertical air movements over the YRD region are not restricted at the lower atmosphere any more. As shown in Fig. 7~~6~~d-~~-f~~e ~~and 8d-e~~ f ~~(August 10 and 11)~~, there are stronger downward airflows from the surface to the top of troposphere. As discussed in Sect. 3.2, ~~SH, HZ, and NJ~~the YRD cities are at the front of the moving typhoon system, so the peripheral circulation of Typhoon Utor may enhance the sinking of atmosphere, which can lead to higher air temperature, lower humidity, and stronger solar radiation. Affected by the enhanced downward air movement as well as the relevant changes of meteorological conditions, O_3 concentrations over the YRD region maintain a high pollution level, with the O_3 concentrations over 60 ppb below the height of 1.5 km (Fig. 7d-f). Furthermore, ~~as shown in Fig. 86d to f,~~ the high value center of O_3 concentrations ~~above~~ (>90 ppb) moves ~~from southeast to north~~westwards during August 10-12, implying that the peripheral circulation of Typhoon Utor can drive the air from the coastal areas to the inland areas.

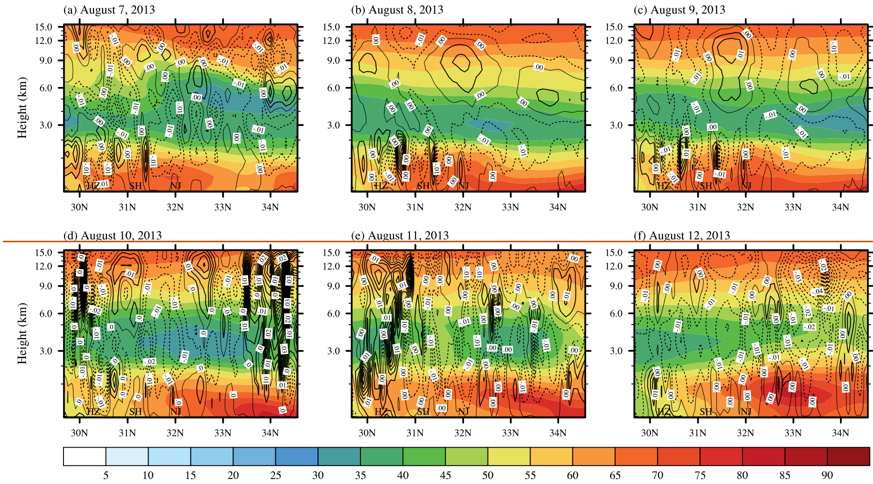

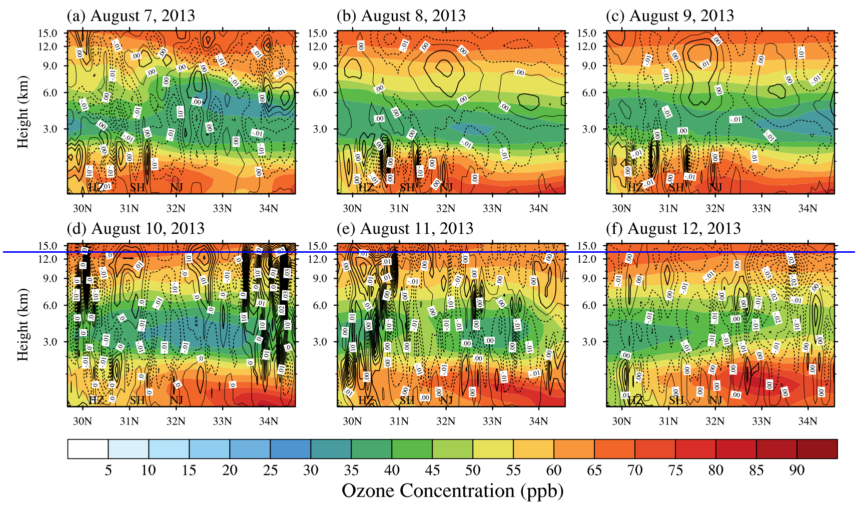

Fig. 67. Simulated daytime vertical wind velocity and vertical distribution of O_3 concentrations in the YRD region from 29.67°E N to 34.76°E N during August 7 to 12 2013, with the values averaged in the meridional direction from 118°E to 122°E. The marks of HZ, SH, and NJ point out the latitudes of Hangzhou, Shanghai, and Nanjing, respectively. The solid lines show the zero velocity lines or positive wind speeds and represent upward airflow, while the dotted lines show the negative wind speeds and represent downward airflow. (anThe interval isof 0.005 m/s).

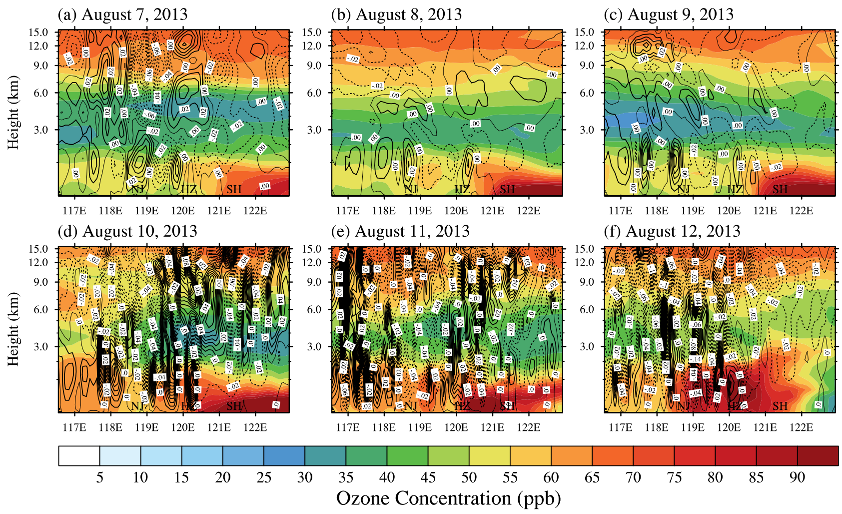

Fig. 78. Simulated daytime vertical wind velocity and vertical distribution of O_3 concentrations from 116.5°E to 122.9°E during August 7 to 12 2013 at the zonal directionalong the latitude of 31.40°N, (where Shanghai site lieis locatesd) during August 7 to 12 2013. The marks of SH HZ, SHHZ and NJ point out the longitudes of Shanghai Hangzhou, HangzhouShanghai, and Nanjing, respectively. The dotted lines show the negative wind speeds and represent downward airflow, while the solid lines show the zero velocity lines orthe positive wind speeds and represent upward airflow zero vertical velocity, while the dotted lines show the negative wind speeds and represent downward airflow. (anThe interval ofis 0.01 m/s).

带格式的：居中

The vertical changes of wind velocity and O_3 concentrations above Shanghai, Hangzhou and Nanjing are further illustrated in Fig. 897. Similarly to that in Fig. 67 and 8, the atmospheric subsidence can also be found in the boundary layertroposphere of Shanghai and Hangzhou (Fig. 97a and b) (usually occur at more than 1 km above the surface) during the period of the high-level O_3 pollution (from August 7 to 12 August). ForWith respect to Shanghai site, aAffected by the extremely high temperature, more active photochemical reactions lead to higher O_3 concentrations in the whole atmospheric boundary layer. The downward airflows induced by the subtropical high trap and enhance the accumulation of surface O_3 as time passes. Thus, high O_3 concentrations are formed below 2 km above the urban areas of Shanghai, and the high concentration centers occur near the surface below 500 m. It is interesting that O_3 concentration on August 8 is comparatively lower, which can be seen in Fig. 2 as well. This phenomenon can be explained by the fact shown in Fig. 97a that the transient upward airflow occurs at above 300 m over Shanghai and inhibits the accumulation of the O_3 pollution at the surface (shown in Fig. 8a). Additionally, Fig. 897a also presents the possible effects of Typhoon Utor on the formation of O_3. On August 10, when the typhoon system approaches to the eastern coastal areas of China, the sinking air above Shanghai is apparently strengthened, and thereby enhances the intensity of O_3 pollution as well as the scope of the pollution. But after August 12, when Typhoon Utor changes the wind and even impacts the subtropical high, high temperature is alleviated and the build-up O_3 is transported to other places. Thus, the pollution is mitigated. As to

~~As for~~ Hangzhou~~-site~~ (Fig. ~~7~~98b), from August 7 to 9, owing to weaker photochemical reactions, lower O_3 concentrations than that in Shanghai are found in the boundary layer~~-owing to weaker photochemical reaction, while much more remarkable atmospheric subsidence is observed above Hangzhou, indicating that massive chemical formation is important for vertical transport process in the high O_3-episodes~~. However, the O_3 concentration can exceeds the national standard from August 10 to 12 (Fig. 2), which should be influenced by the typhoon system. The influence process is similar to the above discussion for Shanghai, that is, the upper downward airflows (over 1 km above the surface) are enhanced significantly since August 10. ~~The over-standard of O_3 concentration can be attributed to the strengthened chemical formation, as well as the enhanced vertical transport process. The influence by the typhoon system is similar to the above discussion for Shanghai, as the downward air flow is enhanced significantly since August 10.~~

~~As demonstrated in Fig. 89c~~But for Nanjing, the O_3 concentration does not exceed the national O_3 standard during August 7-12 (Fig.2 and 8), which should be attributed to the fact that Nanjing is far away from the coastal areas and thereby hardly affected by the downward flow in the typhoon periphery. Though the O_3 concentration in Nanjing increases on August 12, it should mainly be caused by the local photochemical reactions because the vertical movement below 2 km above Nanjing is dominated by upward airflows.

带格式的：下标

~~the vertical O_3-concentration distribution and vertical velocity at Nanjing site show differences. The O_3-concentrations below boundary layer is substantially lower than that of Shanghai and Hangzhou. Besides, from August 7 to 10, vertical velocity is found extremely weak near the ground, as massive zero-velocity lines appear below 500 m. From August 11 to 12, although the O_3-concentration is increasing as the high center is upper at the altitude of around 1 km. But, the vertical movement below 2 km is dominated by upward airflow, thus the surface O_3 pollution is relieved with the O_3-concentration lower than the national standard (Fig. 2).~~

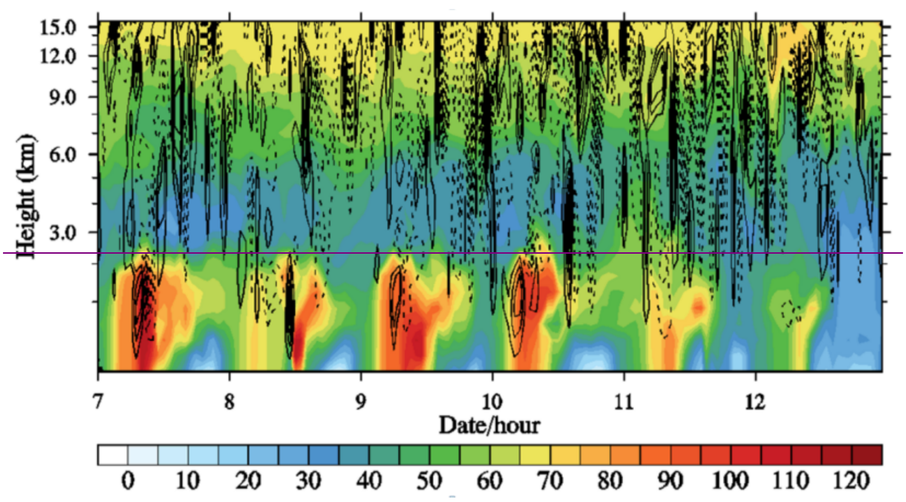

Height (km)
15.0
12.0
9.0
6.0
3.0
7
8
9
10
11
12
Date/hour
0
10
20
30
40
50
60
70
80
90
100
110
120

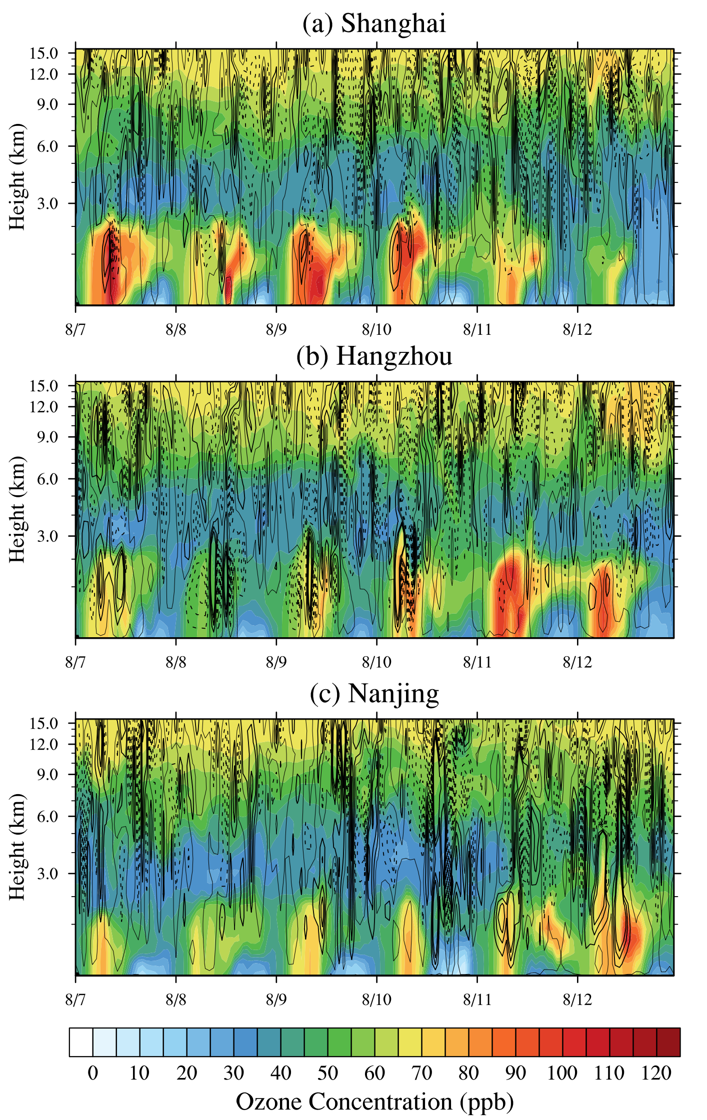

Fig. ~~7~~89. Temporal variations of the vertical wind velocity and the vertical distribution of O_3 concentrations above (a) Shanghai, (b) Hangzhou and (c) Nanjing during August 7 to 12 2013. The dotted lines show the negative wind speeds and represent the downward airflows, while the solid lines show ~~the zero-velocity lines or~~ the positive wind speeds– and zero vertical velocity.~~represent upward airflow, while the dotted lines show the negative wind speeds and represent downward air flow (an~~ The interval ~~of~~is 0.005 m/s~~)~~.

It is also should be mentioned that the near-surface vertical velocities around these cities are much lower than those at higher altitudes (Fig.8). Especially in the planetary boundary layer (< 1 km), lots of zero-velocity lines appear near the ground. This phenomenon may be related with the upward airflow caused by Urban Heat Islands. Thus, the maximum centers of O_3 occur near the surface below 500 m, and the vertical diffusion process plays a more important role in the

带格式的: 下标

accumulation of surface O_3. The essential role of the vertical diffusion process in the O_3 episode is similar to that reported by Zhu et al. (2015).

带格式的：下标

带格式的：下标

~~**Shanghai (SH) during August 7 to 12, 2013.**~~

4.3 Process analysis for ozone formation

4.3.1 Typical cities in the YRD region

Fig. ~~8~~109 shows the ~~da~~daytime~~ily~~ contributions of different atmospheric processes to the formation of O_3 in Shanghai (SH), Nanjing (NJ), and Hangzhou (HZ) at the first modeling layer from August 4 to 15 ~~August~~ 2013. As shown in the figure, for all cities during this period, the major contributors to high O_3 concentrations include the vertical diffusion (VDIF), the dry deposition (DDEP), the gas-phase chemistry (CHEM), and the total advection (TADV). TADV is the sum of the horizontal advection (HADV) and the vertical advection (ZADV). In this study, HADV and ZADV are considered together as TADV because they are inevitably linked as the inseparable parts of air circulation. As discussed in Sect. 3.2, the strong sinking air causes slow wind on the ground and little clouds in the sky, so the contributions of horizontal diffusion (HDIF) and cloud processes (CLDS) are quite small during this episode.

In the first layer of the urban areas of Shanghai (Fig. ~~10~~9~~8~~a), the averaged ~~daily daytime~~ contributions from ~~during August 4-15 August for~~ the vertical diffusion (VDIF), the gas-phase chemistry (CHEM), the advection processe~~s~~ (TADV), and the dry deposition (DDEP) during the daytime of August 4-15 are 9.95, 10.10, -11.74 and -7.28 ppb/h, respectively. Obviously, VDIF and CHEM exhibit significant positive contributions to O_3 during most days, while TADV and DDEP mainly show the consumption contributions. The sinking air caused by the weather system discussed in Sect. 3.2 can trap heat and air pollutants on the ground, and ~~results in~~make VDIF ~~to~~ be the most import source of surface O_3. Meanwhile, the hotter and dryer weather with more sunshine, above 40 ^{o}C and comparatively low relative humidity (shown in Fig. 4), which is related with the sinking air, can enhance the photochemical reactions. So, CHEM can form more O_3 on the ground. Compared with the time series of CHEM and DDEP in which there are no obvious fluctuations, the values of VDIF and TADV significantly change with the time, with the ~~daily~~ daytime mean contributions varying from 3.99 to 28.45 ppb/h for VDIF and from -2.56 to -28.13 ppb/h for TADV. These time variations should be related with the changes of vertical air movement. For example, the value of VDIF on August 8 is only 3.99 ppb/h, which can be attributed to the local transient upward airflow over Shanghai (shown in Fig. 98a7). On August 10, however, VDIF can contribute 28.45 ppb O_3 per hour, which may be related with the enhanced downward air movement caused by the peripheral circulation of Typhoon Utor. Moreover, during the high-level O_3 episode from August 7-12, the mean values for VDIF, CHEM, TADV and DDEP are 13.41, 11.21, -8.37 and -14.74 ppb/h. But after August 12, the mean contributions of VDIF, CHEM, TADV and DDEP decrease to 5.35, 9.53, -5.52 and -10.85 ppb/h. These reductions should be related with the process that the subtropical high moves eastward and northward forced by Typhoon Utor (Fig. 5d). By quantifying the relative importance of each process to O_3 formation, the IPR analysis provides a fundamental explanation for the synthetically influence of the high pressure and the typhoon system, which has been discussed in Sect. 3.2 and 4.1, and further illustrates the exact mechanism.

Fig. 8109b presents the result of IPR analysis for Hangzhou. During August 4-15, VDIF and CHEM are the major source of surface O_3 with the average contribution of 5.36 ppb/h for VDIF and 10.97 ppb/h for CHEM, while TADV and DDEP are two important sinks for O_3 with the average contribution of -9.63 ppb/h for TADV and -5.14 ppb/h for DDEP. Synthetically impacted by Western Pacific subtropical high and Typhoon Utor, the mean contributions during the O_3 episode (from August 7 to August 12) for VDIF, CHEM, TADV and DDEP increase to 7.21, 12.61, -11.51 and -5.92 ppb/h, respectively. The highest VDIF contribution occurs on August 10-11, and the over-standard of O_3 concentration appears on August 10-12 as well, which may be attributed to the effect of typhoon's peripheral circulation, implying Typhoon Utor also plays an essential role in the formation of O_3 pollution in Hangzhou. After Typhoon Utor approaches close enough to Hangzhou, the wind direction is mainly dominated by the southeast wind (Fig. 4b), and the mean values of VDIF, CHEM, TADV and DDEP finally decrease to 4.84, 10.08, -8.92 and -4.78 ppb/h, respectively. In a word, Hangzhou is located close to Shanghai, so the temporal variations of VDIF, CHEM, TADV and DDEP in Hangzhou are similar to those in Shanghai.

However, the similar variation pattern of VDIF, CHEM, TADV and DDEP occurring in Shanghai and Hangzhou does not appear in Nanjing. As shown in Fig. 8109c, the mean contributions of VDIF, CHEM, TADV and DDEP to surface O_3 in Nanjing are 11.31, 9.55 -1.34 and -17.57 ppb/h during the whole period, while the values during 7-12 August are 10.32, 10.70,

-0.99 and -18.42 ppb/h. There are no apparent fluctuations or sudden increases of these contributors during the period from August 4 to 15, so are the O_3 concentration (Fig. 2), temperature and relative humidity (Fig. 4a), implying Nanjing is generally under the control of the Western Pacific subtropical high and can hardly be affected by the typhoon system. ~~The above discussion in Section 4.2 also proved this conclusion.~~ As a typical city in the northwest inland area of the YRD region (NIR), Nanjing is located far away from the sea, which means it may not be easily affected by the peripheral circulation of the typhoon system~~weather system from the ocean~~.

Additionally, at the altitude of 500 m and 1500 m above Shanghai, Nanjing, and Hangzhou (not shown), CHEM is also the major contributor to O_3 formation, with the values a litter lower than those at the surface, suggesting that there are strong photochemical reactions in the whole boundary layer of these YRD cities. In contrast, VDIF has an opposite effect in the middle of the boundary layer, with the negative contributions for O_3 of -3.26 ppb/h in Shanghai, -2.37 ppb/h in Hangzhou, and -3.21 ppb/h in Nanjing, respectively (not shown). The loss of O_3 at higher atmospheric level caused by VDIF further proves the essential role of the downward vertical movement in this O_3 episode.

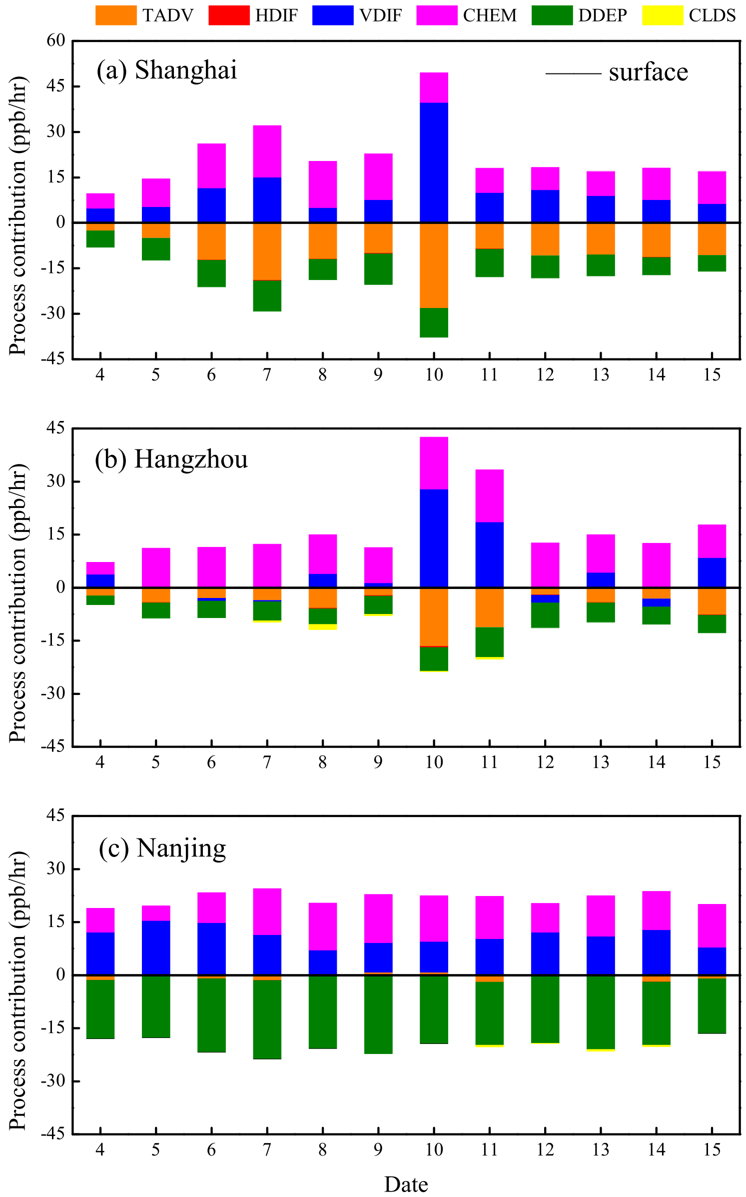

Fig. ~~8~~9~~10~~. Variations of the ~~daily~~ daytime mean values for the contributions of individual processes to O_3 formation in (a) Shanghai, (b) Hangzhou, and (c) Nanjing from August 4 to 15 ~~August~~ 2013 at the surface layer. The contributors include the total advection (TADV), the horizontal diffusion (HDIF), the vertical diffusion (VDIF), the gas-phase chemistry (CHEM), the dry deposition (DDEP), and the cloud processes with the aqueous chemistry (CLDS).

4.3.2 Spatial distribution of the contributors for the O_3 episode over the YRD region

Fig. ~~9~~ 10 demonstrates the spatial distribution of the mean contributions of main processes

(VDIF, CHEM, DDEP and TADV) to the ozone formation~~ of this high-level O_3 episode~~ at the lowest modeling layer in domain 3 during this high-level O_3 episode. The modeling results from 7 to 12 August are averaged to provide the mean values.

Similar to the results shown in Fig. ~~8~~9, Fig. ~~9~~10 illustrates that the vertical diffusion (VDIF) and the gas-phase chemistry (CHEM) exhibit significant positive contributions to O_3 over the YRD region and the surrounding areas during the high-level O_3 episode. The contributions of VDIF in domain 3 (Fig. 10~~9~~a) range from 5 to 25 ppb/h, with the high values (> 20 ppb/h) occurring in the southeast coastal areas. For CHEM (Fig. 10~~9~~b), the contributions vary within the range of 0-15 ppb/h, with the high values over 10 ppb/h appearing in and around the big cities. As discussed above, these regional positive contributions of VDIF and CHEM over domain 3 should be related to the facts that the whole region is under the control of the Western Pacific subtropical high. With respect to the higher contributions of CHEM in the urban areas, they should be attributed to the spatial distribution of the emissions of O_3 precursors, which is also higher in the cities. Furthermore, higher air temperature in the cities related with the urban heat island may enhance the chemical reactions and form more O_3 in these areas as well.

~~As shown in Fig. 9e,~~ For DDEP, it is the main critical factor of the consumption of O_3, with the negative contributions varying from 0 to -25 ppb/h over the modeling domain 3 (Fig. 10c). Small values usually occur on the water, which may be related with less air pollution over rivers, lakes and oceans. High values can be found on land, especially in the southeast coastal areas. For the contributions of TADV~~ (Fig. 9d)~~, the values in domain 3 range from -10 to 10 ppb/h, with the positive contributions generally occurring on land while the negative ~~(consuming)~~ ones appearing on the water (Fig. 10d). The maximum positive contributions of TADV are usually found along the boundary between the land and the water, which should be explained by the facts that the land-sea breeze circulations can play an important role in the redistribution of the formed O_3. On account of the high-pressure system and so-caused sinking airflows in the YRD region, the background wind is relatively weak in comparison to the local atmospheric circulation, thus the sea breeze can easily bring more generated O_3 to the seashore.

~~From the discussion in Section 3 and 4.2~~

~~In all, more active photochemical reactions and the vertical diffusion play a significant role in~~

the accumulation of surface O_3, and lead to the high-level O_3 pollution episode over the YRD region. The major driving factor should be the Western Pacific subtropical high. Moreover, the changes in the contributions of VDIF, CHEM, DDEP, and TADV between August 7-9 and August 10-12 CHEM exhibit a similar spatial pattern with the high values and increased values mostly concentrate concentrating in the southeast coastal areas (Fig. 12), implying the Typhoon Utor also plays a collaborative effect, which is clearly shown in Fig. 13. The details and the processes of the synthetical effects of high pressure and typhoon system have been discussed in Sect. 3.2, 4.2 and 4.3.1 as well.

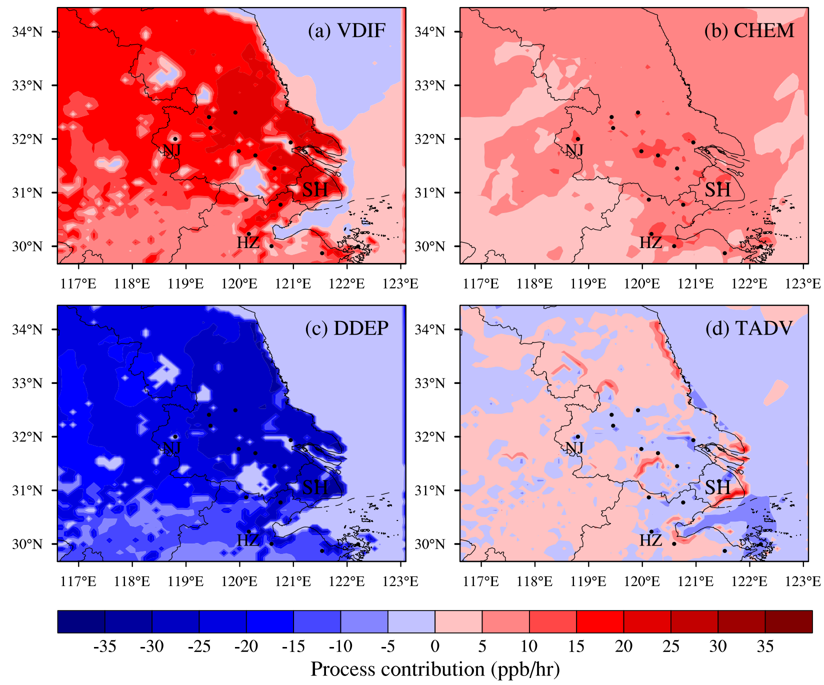

Fig. 9. The contributions of main processes to O_3 formation over the YRD region, including (a) vertical diffusion (VDIF), (b) gas chemistry (CHEM), (c) dry deposition (DDEP), and (d) total advection (TADV). The values are averaged from August 7 to 12 2013.

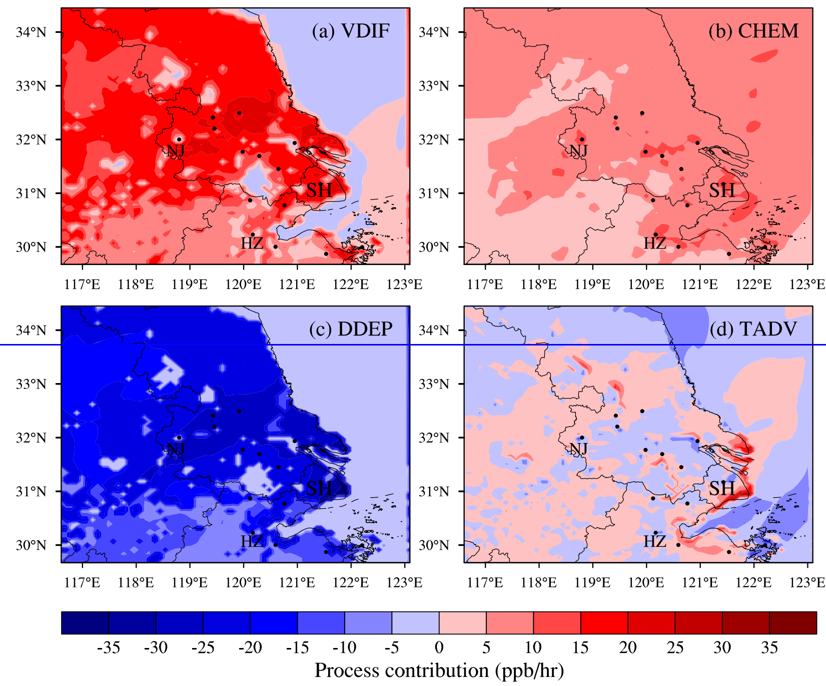

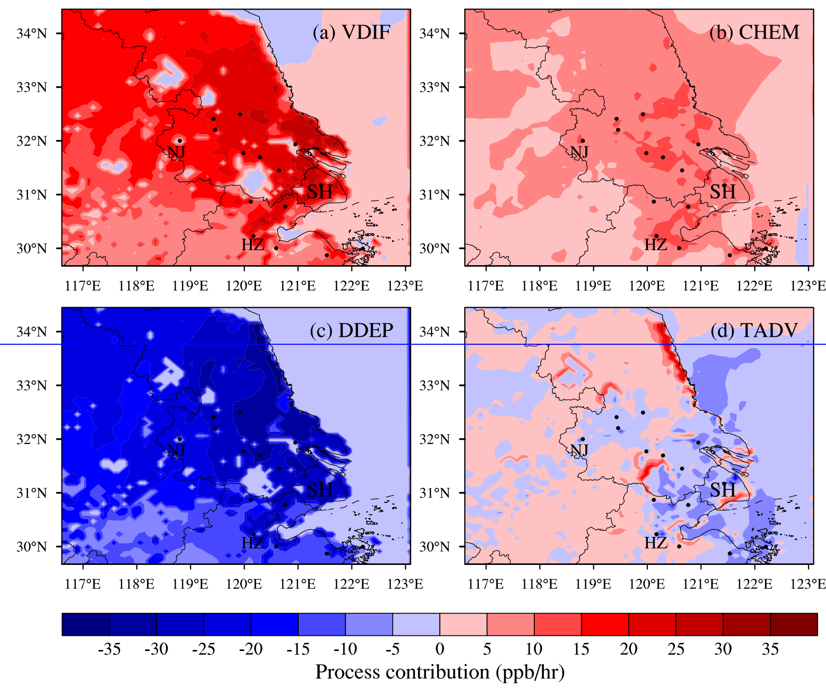

Fig. 12. The daytime contributions of main processes to O_3 formation over the YRD region, including (a) vertical diffusion (VDIF), (b) gas chemistry (CHEM), (c) dry deposition (DDEP), and (d) total advection

(TADV). The values are averaged from August 10 to 12 2013.

From the discussion in Section 3 and 4.2, it can be deduced that typhoon Utor plays an important role in the formation of ozone over the YRD region during August 10-12. To clearly clarify the effect of the typhoon system in this O_3 pollution episode, we firstly average the modeling results of VDIF, CHEM, DDEP and TADV during August 10-12 to show their contributions to O_3 formation when the typhoon system plays an important role. Secondly, the modeling results of these processes from August 7 to 9 are also averaged to provide their contributions when only the subtropical high dominates the episode. Finally, the differences of the contributions of VDIF, CHEM, DDEP and TADV between the period of August 7-9 and August 10-12 are calculated to reveal the role of the typhoon system in this severe high O_3 episode (Fig. 11). As shown in Fig. 11a, when YRD is affected by the peripheral circulation of Typhoon Utor, the contributions of VDIF over the YRD region increase by 0-15 ppb/h, with the higher increment values (> 30 ppb/h) occurring in the southeast coastal region (SCR) and center inland region (CIR), implying that SCR and CIR can be largely affected by the peripheral subsidence airflows of the typhoon system. As to the contributions of CHEM, the increases caused by the typhoon system are 0-5 ppb/h over the YRD region, and the higher increment also appears in the coastal areas (Fig. 11b). For DDEP, influenced by typhoon Utor, its negative contributions decrease up to -20 ppb/h, with the largest reduction along the coastline (Fig. 11c). For TADV, with the approaching of typhoon Utor, the contributions of TADV particularly decrease by 0-20 ppb/h, especially in the southeast coastal region (Fig. 11d).

In all, during this high-level O_3 pollution episode, more active photochemical reactions and the vertical diffusion play a significant role in the accumulation of surface O_3 over the YRD region. The major driving factor should be the Western Pacific subtropical high. Moreover, the changes in the contributions of VDIF, CHEM, DDEP, and TADV between August 7-9 and August 10-12 exhibit a similar spatial pattern with the high values mostly concentrating in the southeast coastal areas (Fig. 12), implying the Typhoon Utor also plays a collaborative effect.

带格式的: 下标

带格式的: 下标

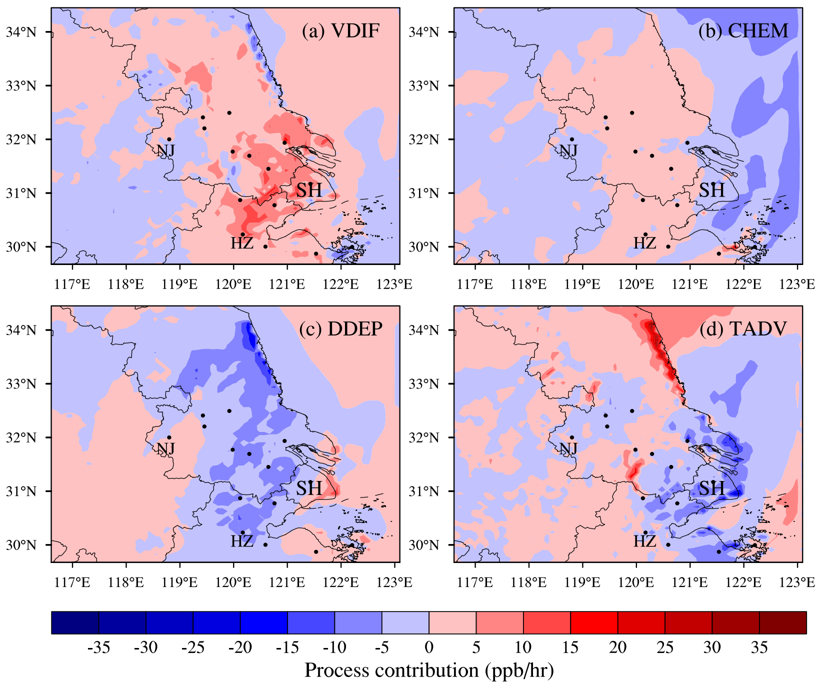

Fig. 1~~3~~1. The difference of daytime mean contributions of main processes to O_3 formation over the YRD region between the period of August 10-12 and August 7-9~~between~~ , including (a) vertical diffusion (VDIF), (b) gas chemistry (CHEM), (c) dry deposition (DDEP), and (d) total advection (TADV) ~~between the period of August 7-9 and August 10-12 (values averaged from August 10-12 minus that of August 7-9)~~.

5. Conclusions

In this study, ~~By means of observational analysis and numerical simulation,~~ the characteristics and the essential impact factors of a typical regional continuous O_3 pollution over the YRD region is investigated by means of observational analysis and numerical simulation. ~~Base on the observation data, it is found that this high-level O_3~~The episode lasted~~s~~ for nearly a week from August 7 to 12 ~~August~~ 2013, with the O_3 concentration exceeding the national air quality standard in more than half of the cities over the YRD region. ~~In the cities of Jiaxing, Changzhou and Nantong, high O_3 concentrations can reach the values over 160 ppb. Fine weather conditions, such as extremely high temperature, low relative humidity, and weak wind speed, provide a favorable atmospheric environment for the complicated photochemical reactions and help to form O_3.~~ The analysis of weather systems and the modeling results from WRF/CMAQ all illustrate that the continuous strong Western Pacific subtropical high is the leading factor of the abnormally high temperature weather and the heavy O_3 pollution, by inducing more sinking air to trap heat as well as air pollutants at the surface. Meanwhile, ~~T~~the development of this episode is closely related to the movement of Typhoon Utor as well. The temporal variations of the vertical wind velocity and O_3 concentrations show that when the YRD region is at the front of moving typhoon system, the downward airflow is enhanced in the boundary layer with fine weather, and thereby the air pollutants are trapped and accumulated near the surface. Moreover, in the last stage of the O_3 episode, the activity of Typhoon Utor weakens the strength of the subtropical high and forces it to retreat easterly and move northward, and the prevailing southeasterly surface wind related with the approaching of Typhoon Utor contributes to the mitigation of the O_3 pollution.

The Integrated Process Rate (IPR) analysis implemented in CMAQ is specially carried out to quantify the relative contributions of individual processes and give a fundamental explanation. ~~Over the YRD region, D~~During the high-level O_3 episode from August 7-12, the vertical diffusion (VDIF) and the gas-phase chemistry (CHEM) exhibit significant positive contributions to surface O_3~~,~~ over the YRD region, ~~–~~with the high values over 20 ppb/h for VDIF and over 10 ppb/h for CHEM. The dry deposition (DDEP) is the major sink of surface O_3, while ~~T~~the total advection (TADV) can give the positive contribution on land and the negative contribution on the water. ~~The dry deposition (DDEP) is the major sink of surface O_3, while the contributions of horizontal diffusion (HDIF) and cloud processes (CLDS) are quite small. To some extent, the distribution pattern reflects the heterogeneity of emissions and the effects of weather system. Influenced by the sinking air as well as the fine weather induced by the Western Pacific subtropical high, the contributions of VDIF and CHEM to surface O_3 maintain the high values of 13.41 and 11.21 ppb/h for Shanghai, 7.21 and 12.61 ppb/h for Hangzhou, and 10.32 and 10.70 ppb/h for Nanjing, respectively.~~ Moreover, on August 10-~~11~~12, the YRD region~~cities close to the sea are~~ is apparently affected by the periphery circulation of Typhoon Utor, with the contributions of VDIF over the YRD region increas~~e~~ing by 0-15 ppb/h, the contributions of CHEM increasing by 0-5 ppb/h, and the contributions of DDEP and TADV decreasing. Especially in the coastal cities, such as Shanghai and Hangzhou, the effects of the typhoon system are more obvious. ~~particularly an increase to 28.45 ppb/h in Shanghai and 19.76 ppb/h in Hangzhou. Meanwhile, the contributions of CHEM in YRD increase by 0-5 ppb/h, while the negative contributions of DDEP decrease by 0-20 ppb/h with large decrease values appear along the coastline.~~ In contrast, the cities in the northwest inland area– of the YRD region, ~~(NIR)~~ which are far away from the sea, ~~are generally under the control of the subtropical high and~~ can hardly be affected by the typhoon system ~~owing to the location far away from the sea~~. In the end, ~~W~~when the typhoon– system significantly weakens the high pressure system, the contributions of VDIF, CHEM, TADV, and DDEP decrease to a low level in all cities.

WRF/-CMAQ model system shows a relatively good performance in simulation of the O_3 episode, with the simulated meteorological conditions and air pollutant concentrations basically in agreement with the observations in most YRD cities. Our results in this study can provide an insight for the formation mechanism of regional O_3 pollution in East Asia, and help to forecast the O_3 pollution synthetically impacted by the Western Pacific subtropical high and the tropical cyclone system.

Acknowledgments

This study was supported by the National Natural Science Foundation of China (41475122, 91544230, 41575145), the National Special Fund for Environmental Protection Research in the Public Interest (201409008), EU 7th Framework Marie Curie Actions IRSES project REQUA (PIRSES-GA-2013-612671), and the National Science Foundation of Jiangsu Provence (BE2015151). The authors would like to thank Hongli Wang from Shanghai Academy of Environmental Sciences for providing VOCs observation data, Xiaoxun Xie for preliminary data processing, and the anonymous reviewers for their constructive and precious comments on this manuscript.

References

An, X., Zhu, T., Wang, Z., Li, C., and Wang, Y.: A modeling analysis of a heavy air pollution episode occurred in Beijing, Atmos Chem Phys, 7, 3103-3114, 2007.

Byun, D., and Schere, K. L.: Review of the governing equations, computational algorithms, and other components of the models-3 Community Multiscale Air Quality (CMAQ) modeling system, Appl Mech Rev, 59, 51-77, 10.1115/1.2128636, 2006.

Chan, C. K., and Yao, X.: Air pollution in mega cities in China, Atmos Environ, 42, 1-42, 10.1016/j.atmosenv.2007.09.003, 2008.

Chen, F., and Dudhia, J.: Coupling an advanced land surface-hydrology model with the Penn State-NCAR MM5 modeling system. Part I: Model implementation and sensitivity, Mon Weather Rev, 129, 569-585, Doi 10.1175/1520-0493(2001)129<0569:Caalsh>2.0.Co;2, 2001.

Chen, D., Zhou, B., Beirle, S., Chen, L. M., and Wagner, T.: Tropospheric NO2 column densities deduced from zenith-sky DOAS measurements in Shanghai, China, and their application to satellite validation, Atmos Chem Phys, 9, 3641-3662, 2009.

Cheng, W. L., Lai, L. W., Den, W., Wu, M. T., Hsueh, C. A., Lin, P. L., Pai, C. L., and Yan, Y. L.: The relationship between typhoons' peripheral circulation and ground-level ozone concentrations in central Taiwan, Environ Monit Assess, 186, 791-804, 10.1007/s10661-013-3417-7, 2014.

Chiqueto, J., Silva, M. E. S.: São Paulo "Surface Ozone Layer" and the atmosphere: characteristics of tropospheric ozone concentrations in the city and how the atmosphere influences them, VDM Verlag Dr. Muller, Saarbrücken, 2010.

Ding, A. J., Fu, C. B., Yang, X. Q., Sun, J. N., Zheng, L. F., Xie, Y. N., Herrmann, E., Nie, W., Petaja, T., Kerminen, V. M., and Kulmala, M.: Ozone and fine particle in the western Yangtze River Delta: an overview of 1 yr data at the SORPES station, Atmos Chem Phys, 13, 5813-5830, 10.5194/acp-13-5813-2013, 2013.

Duan, J. C., Tan, J. H., Yang, L., Wu, S., and Hao, J. M.: Concentration, sources and ozone formation potential of volatile organic compounds (VOCs) during ozone episode in Beijing, Atmos Res, 88, 25-35, 10.1016/j.atmosres.2007.09.004, 2008.

Emmons, L. K., Walters, S., Hess, P. G., Lamarque, J. F., Pfister, G. G., Fillmore, D., Granier, C., Guenther, A., Kinnison, D., Laepple, T., Orlando, J., Tie, X., Tyndall, G., Wiedinmyer, C., Baughcum, S. L., and Kloster, S.: Description and evaluation of the Model for Ozone and Related chemical Tracers, version 4 (MOZART-4), Geosci Model Dev, 3, 43-67, 2010.

Fann, N., and Risley, D.: The public health context for PM2.5 and ozone air quality trends, Air Qual Atmos Hlth, 6, 1-11, 10.1007/s11869-010-0125-0, 2013.

Feng, Z. W., Jin, M. H., Zhang, F. Z., and Huang, Y. Z.: Effects of ground-level ozone (O-3) pollution on the yields of rice and winter wheat in the Yangtze River Delta, J Environ Sci-China, 15, 360-362, 2003.

Foley, K. M., Roselle, S. J., Appel, K. W., Bhave, P. V., Pleim, J. E., Otte, T. L., Mathur, R., Sarwar, G., Young, J. O., Gilliam, R. C., Nolte, C. G., Kelly, J. T., Gilliland, A. B., and Bash, J. O.: Incremental testing of the Community Multiscale Air Quality (CMAQ) modeling system version 4.7, Geosci Model Dev, 3, 205-226, 2010.

Gao, J. H., Bin, Z., Xiao, H., Kang, H. Q., Hou, X. W., and Shao, P.: A case study of surface ozone source apportionment during a high concentration episode, under frequent shifting wind conditions over the Yangtze River Delta, China, Sci Total Environ, 544, 853-863, 10.1016/j.scitotenv.2015.12.039, 2016.

Geng, F. H., Tie, X. X., Xu, J. M., Zhou, G. Q., Peng, L., Gao, W., Tang, X., and Zhao, C. S.: Characterizations of ozone, NOx, and VOCs measured in Shanghai, China, Atmos Environ, 42, 6873-6883, 10.1016/j.atmosenv.2008.05.045, 2008.

Goncalves, M., Jimenez-Guerrero, P., and Baldasano, J. M.: Contribution of atmospheric processes affecting the dynamics of air pollution in South-Western Europe during a typical summertime photochemical episode, Atmos Chem Phys, 9, 849-864, 2009.

Grell, G. A., and Devenyi, D.: A generalized approach to parameterizing convection combining ensemble and data assimilation techniques, Geophys Res Lett, 29, Artn 169310.1029/2002gl015311, 2002.

Guo, H., Jiang, F., Cheng, H. R., Simpson, I. J., Wang, X. M., Ding, A. J., Wang, T. J., Saunders, S. M., Wang, T., Lam, S. H. M., Blake, D. R., Zhang, Y. L., and Xie, M.: Concurrent observations of air pollutants at two sites in the Pearl River Delta and the implication of regional transport, Atmos Chem Phys, 9, 7343-7360, 2009.

Han, S. Q., Bian, H., Feng, Y. C., Liu, A. X., Li, X. J., Zeng, F., and Zhang, X. L.: Analysis of the Relationship between O-3, NO and NO2 in Tianjin, China, Aerosol Air Qual Res, 11, 128-139, 10.4209/aaqr.2010.07.0055, 2011.

Hong, S. Y., Dudhia, J., and Chen, S. H.: A revised approach to ice microphysical processes for the bulk parameterization of clouds and precipitation, Mon Weather Rev, 132, 103-120, Doi 10.1175/1520-0493(2004)132<0103:Aratim>2.0.Co;2, 2004.

Hong, S. Y., Noh, Y., and Dudhia, J.: A new vertical diffusion package with an explicit treatment of entrainment processes, Mon Weather Rev, 134, 2318-2341, Doi 10.1175/Mwr3199.1, 2006.

Huang, J. P., Fung, J. C. H., Lau, A. K. H., and Qin, Y.: Numerical simulation and process analysis of typhoon-related ozone episodes in Hong Kong, J Geophys Res-Atmos, 110, Artn D0530110.1029/2004jd004914, 2005.

Huang, J. P., Fung, J. C. H., and Lau, A. K. H.: Integrated processes analysis and systematic meteorological classification of ozone episodes in Hong Kong, J Geophys Res-Atmos, 111, Artn D2030910.1029/2005jd007012, 2006.

Hung, C. H., and Lo, K. C.: Relationships between Ambient Ozone Concentration Changes in Southwestern Taiwan and Invasion Tracks of Tropical Typhoons, Adv Meteorol, Artn 40297610.1155/2015/402976, 2015.

Jenkin, M. E., and Clemitshaw, K. C.: Ozone and other secondary photochemical pollutants: chemical processes governing their formation in the planetary boundary layer, Atmos Environ, 34, 2499-2527, Doi 10.1016/S1352-2310(99)00478-1, 2000.

Jiang, F., Wang, T. J., Wang, T. T., Xie, M., and Zhao, H.: Numerical modeling of a continuous photochemical pollution episode in Hong Kong using WRF-chem, Atmos Environ, 42, 8717-8727, 10.1016/j.atmosenv.2008.08.034, 2008.

Jiang, F., Zhou, P., Liu, Q., Wang, T. J., Zhuang, B. L., and Wang, X. Y.: Modeling tropospheric ozone formation over East China in springtime, J Atmos Chem, 69, 303-319, 10.1007/s10874-012-9244-3, 2012.

Kim, H. J., and Wang, B.: Sensitivity of the WRF Model Simulation of the East Asian Summer Monsoon in 1993 to Shortwave Radiation Schemes and Ozone Absorption, Asia-Pac J Atmos Sci, 47, 167-180, 10.1007/s13143-011-0006-y, 2011.

Lam, K. S., Wang, T. J., Wu, C. L., and Li, Y. S.: Study on an ozone episode in hot season in Hong Kong and transboundary air pollution over Pearl River Delta region of China, Atmos Environ, 39, 1967-1977, 10.1016/j.atmosenv.2004.11.023, 2005.

Landry, J. S., Neilson, E. T., Kurz, W. A., and Percy, K. E.: The impact of tropospheric ozone on landscape-level merchantable biomass and ecosystem carbon in Canadian forests, Eur J Forest Res, 132, 71-81, 10.1007/s10342-012-0656-z, 2013.

Li, L., Chen, C. H., Huang, C., Huang, H. Y., Zhang, G. F., Wang, Y. J., Chen, M. H., Wang, H. L., Chen, Y. R., Streets, D. G., and Fu, J. M.: Ozone sensitivity analysis with the MM5-CMAQ modeling system for Shanghai, J Environ Sci-China, 23, 1150-1157, 10.1016/S1001-0742(10)60527-X, 2011.

Li, L., Chen, C. H., Huang, C., Huang, H. Y., Zhang, G. F., Wang, Y. J., Wang, H. L., Lou, S. R., Qiao, L. P., Zhou, M., Chen, M. H., Chen, Y. R., Streets, D. G., Fu, J. S., and Jang, C. J.: Process analysis of regional ozone formation over the Yangtze River Delta, China using the Community Multi-scale Air Quality modeling system, Atmos Chem Phys, 12, 10971-10987, 10.5194/acp-12-10971-2012, 2012.

Li, M. M., Song, Y., Huang, X., Li, J. F., Mao, Y., Zhu, T., Cai, X. H., and Liu, B.: Improving mesoscale modeling using satellite-derived land surface parameters in the Pearl River Delta region, China, J Geophys Res-Atmos, 119, 6325-6346, 10.1002/2014JD021871, 2014.

Li, M. M., Song, Y., Mao, Z. C., Liu, M. X., and Huang, X.: Impacts of thermal circulations induced by urbanization on ozone formation in the Pearl River Delta region, China, Atmos Environ, 127, 382-392, 10.1016/j.atmosenv.2015.10.075, 2016.

Liao, J. B., Wang, T. J., Wang, X. M., Xie, M., Jiang, Z. Q., Huang, X. X., and Zhu, J. L.: Impacts of different urban canopy schemes in WRF/Chem on regional climate and air quality in Yangtze River Delta, China, Atmos Res, 145, 226-243, 10.1016/j.atmosres.2014.04.005, 2014.

Liao, J. B., Wang, T. J., Jiang, Z. Q., Zhuang, B. L., Xie, M., Yin, C. Q., Wang, X. M., Zhu, J. L., Fu, Y., and Zhang, Y.: WRF/Chem modeling of the impacts of urban expansion on regional climate and air pollutants in Yangtze River Delta, China, Atmos Environ, 106, 204-214, 10.1016/j.atmosenv.2015.01.059, 2015.

Liu, X. H., Zhang, Y., Xing, J., Zhang, Q. A., Wang, K., Streets, D. G., Jang, C., Wang, W. X., and Hao, J. M.: Understanding of regional air pollution over China using CMAQ, part II. Process analysis and sensitivity of ozone and particulate matter to precursor emissions, Atmos Environ, 44, 3719-3727, 10.1016/j.atmosenv.2010.03.036, 2010.

Liu, Q., Lam, K. S., Jiang, F., Wang, T. J., Xie, M., Zhuang, B. L., and Jiang, X. Y.: A numerical study of the impact of climate and emission changes on surface ozone over South China in autumn time in 2000-2050, Atmos Environ, 76, 227-237, 10.1016/j.atmosenv.2013.01.030, 2013.

Lou, S. J., Liao, H., and Zhu, B.: Impacts of aerosols on surface-layer ozone concentrations in China through heterogeneous reactions and changes in photolysis rates, Atmos Environ, 85, 123-138, 10.1016/j.atmosenv.2013.12.004, 2014.

Lu, W. Z., and Wang, X. K.: Evolving trend and self-similarity of ozone pollution in central Hong Kong ambient during 1984-2002, Sci Total Environ, 357, 160-168, 10.1016/j.scitotenv.2005.03.015, 2006.

Ma, J. Z., Xu, X. B., Zhao, C. S., and Yan, P.: A review of atmospheric chemistry research in China: Photochemical smog, haze pollution, and gas-aerosol interactions, Adv Atmos Sci, 29, 1006-1026, 10.1007/s00376-012-1188-7, 2012.

Mlawer, E. J., Taubman, S. J., Brown, P. D., Iacono, M. J., and Clough, S. A.: Radiative transfer for inhomogeneous atmospheres: RRTM, a validated correlated-k model for the longwave, J Geophys Res-Atmos, 102, 16663-16682, Doi 10.1029/97jd00237, 1997.

Monin, A. S., Obukhov, A.M.: Basic laws of turbulent mixing in the surface layer of the atmosphere, Contributions of the Geophysical Institute of the Slovak Academy of Sciences 151, 163-187, 1954.

Peng, J. B.: An Investigation of the Formation of the Heat Wave in Southern China in Summer 2013 and the Relevant Abnormal Subtropical High Activities, Atmospheric & Oceanic Science Letters, 7, 286-290, 2014.

Ran, L., Zhao, C. S., Geng, F. H., Tie, X. X., Tang, X., Peng, L., Zhou, G. Q., Yu, Q., Xu, J. M., and Guenther, A.: Ozone photochemical production in urban Shanghai, China: Analysis based on ground level observations, J Geophys Res-Atmos, 114, Artn D1530110.1029/2008jd010752, 2009.

Shao, M., Zhang, Y. H., Zeng, L. M., Tang, X. Y., Zhang, J., Zhong, L. J., and Wang, B. G.: Ground-level ozone in the Pearl River Delta and the roles of VOC and NOx in its production, J Environ Manage, 90, 512-518, 10.1016/j.jenvman.2007.12.008, 2009.

Shi, C. Z., Wang, S. S., Liu, R., Zhou, R., Li, D. H., Wang, W. X., Li, Z. Q., Cheng, T. T., and Zhou, B.: A study of aerosol optical properties during ozone pollution episodes in 2013 over Shanghai, China, Atmos Res, 153, 235-249, 10.1016/j.atmosres.2014.09.002, 2015.

Sillman, S.: The relation between ozone, NOx and hydrocarbons in urban and polluted rural environments, Atmos Environ, 33, 1821-1845, Doi 10.1016/S1352-2310(98)00345-8, 1999.

State Environmental Protection Administration of China: China National Environmental Protection Standard: Automated Methods for Ambient Air Quality Monitoring, China Environmental Science Press, Beijing, 2006.

Tang, W. Y., Zhao, C. S., Geng, F. H., Peng, L., Zhou, G. Q., Gao, W., Xu, J. M., and Tie, X. X.: Study of ozone "weekend effect" in Shanghai, Sci China Ser D, 51, 1354-1360, 10.1007/s11430-008-0088-2, 2008.

Tang, G., Li, X., Wang, Y., Xin, J., and Ren, X.: Surface ozone trend details and interpretations in Beijing, 2001-2006, Atmos Chem Phys, 9, 8813-8823, 2009.

Tu, J., Xia, Z. G., Wang, H. S., and Li, W. Q.: Temporal variations in surface ozone and its precursors and meteorological effects at an urban site in China, Atmos Res, 85, 310-337, 10.1016/j.atmosres.2007.02.003, 2007.

Wang, H. L., Chen, C. H., Wang, Q., Huang, C., Su, L. Y., Huang, H. Y., Lou, S. R., Zhou, M., Li, L., and Qiao, L. P.: Chemical loss of volatile organic compounds and its impact on the source analysis through a two-year continuous measurement, Atmospheric Environment, 80, 488-498, 2013.

Wang, H. X., Zhou, L. J., and Tang, X. Y.: Ozone concentrations in rural regions of the Yangtze Delta in China, J Atmos Chem, 54, 255-265, 10.1007/s10874-006-9024-z, 2006a.

Wang, T. J., Lam, K. S., Xie, M., Wang, X. M., Carmichael, G., and Li, Y. S.: Integrated studies of a photochemical smog episode in Hong Kong and regional transport in the Pearl River Delta of China, Tellus B, 58, 31-40, 10.1111/j.1600-0889.2005.00172.x, 2006b.

Wang, X. M., Lin, W. S., Yang, L. M., Deng, R. R., and Lin, H.: A numerical study of influences of urban land-use change on ozone distribution over the Pearl River Delta region, China, Tellus B, 59, 633-641, 10.1111/j.1600-0889.2007.00271.x, 2007.

Wang, T., Wei, X. L., Ding, A. J., Poon, C. N., Lam, K. S., Li, Y. S., Chan, L. Y., and Anson, M.: Increasing surface ozone concentrations in the background atmosphere of Southern China, 1994-2007, Atmos Chem Phys, 9, 6217-6227, 2009a.

Wang, X. M., Chen, F., Wu, Z. Y., Zhang, M. G., Tewari, M., Guenther, A., and Wiedinmyer, C.: Impacts of Weather Conditions Modified by Urban Expansion on Surface Ozone: Comparison between the Pearl River Delta and Yangtze River Delta Regions, Adv Atmos Sci, 26, 962-972, 10.1007/s00376-009-8001-2, 2009b.

Wei, X. L., Liu, Q., Lam, K. S., and Wang, T. J.: Impact of precursor levels and global warming on peak ozone concentration in the Pearl River Delta Region of China, Adv Atmos Sci, 29, 635-645, 10.1007/s00376-011-1167-4, 2012.

Xie, M., Wang, T.J., Jiang, F., Yang, X.Q.: Modeling of natural NOx and VOC emissions and their effects on tropospheric photochemistry in China, Environ. Sci. China, 28, 31-40, 2007.

Xie, M., Li, S., Jiang, F., and Wang, T. J.: Methane emissions from terrestrial plants over China and their effects on methane concentrations in lower troposphere, Chinese Sci Bull, 54, 304-310, 10.1007/s11434-008-0402-6, 2009.

Xie, M., Zhu, K. G., Wang, T. J., Yang, H. M., Zhuang, B. L., Li, S., Li, M. G., Zhu, X. S., and Ouyang, Y.: Application of photochemical indicators to evaluate ozone nonlinear chemistry and pollution control countermeasure in China, Atmos Environ, 99, 466-473, 10.1016/j.atmosenv.2014.10.013, 2014.

Xie, M., Liao, J., Wang, T., Zhu, K., Zhuang, B., Han, Y., Li, M., Li, S.: Modeling of the anthropogenic heat flux and its effect on regional meteorology and air quality over theYangtze River Delta region, China, Atmos. Chem. Phys., 16, 6071-6089, 10.5194/acp-16-6071-2016, 2016a.

Xie, M., Zhu, K. G., Wang, T. J., Chen, P. L., Han, Y., Li, S., Zhuang, B. L., and Shu, L.: Temporal characterization and regional contribution to O-3 and NOx at an urban and a suburban site in Nanjing, China, Sci Total Environ, 551, 533-545, 10.1016/j.scitotenv.2016.02.047, 2016b.

Yarwood, G., Rao, S., Yocke, M., Whitten G.: Updates to the Carbon Bond chemical mechanism: CB05., Final Report to the U.S. EPA, RT-0400675, 2005.

Zhang, X. Y., Zhang, P., Zhang, Y., Li, X. J., and Qiu, H.: The trend, seasonal cycle, and sources of tropospheric NO2 over China during 1997-2006 based on satellite measurement, Sci China Ser D, 50, 1877-1884, 10.1007/s11430-007-0141-6, 2007.

Zhang, Y. H., Su, H., Zhong, L. J., Cheng, Y. F., Zeng, L. M., Wang, X. S., Xiang, Y. R., Wang, J. L., Gao, D. F., Shao, M., Fan, S. J., and Liu, S. C.: Regional ozone pollution and observation-based approach for analyzing ozone-precursor relationship during the PRIDE-PRD2004 campaign, Atmos Environ, 42, 6203-6218, 10.1016/j.atmosenv.2008.05.002, 2008.

Zhang, Q., Streets, D. G., Carmichael, G. R., He, K. B., Huo, H., Kannari, A., Klimont, Z., Park, I. S., Reddy, S., Fu, J. S., Chen, D., Duan, L., Lei, Y., Wang, L. T., and Yao, Z. L.: Asian emissions in 2006 for the NASA INTEX-B mission, Atmos Chem Phys, 9, 5131-5153, 2009.

Zhu, B., Kang, H. Q., Zhu, T., Su, J. F., Hou, X. W., and Gao, J. H.: Impact of Shanghai urban land surface forcing on downstream city ozone chemistry, J Geophys Res-Atmos, 120, 4340-4351, 10.1002/2014JD022859, 2015.